J. Fluid Mech. (1992), *vol.* 243, *pp.* 103–131
Printed in Great Britain

Asymptotic theory of thermal convection in rapidly rotating systems

By JUN-ICHI YANO†

Theoretische Physik IV, Physikalisches Institut, Universität Bayreuth, Postfach 101251, W-8580 Bayreuth, Germany

(Received 28 June 1991 and in revised form 6 March 1992)

An asymptotic theory of marginal thermal convection in rotating systems is constructed for the limit of rapid rotation. Many self-gravitating astronomical bodies, including the major planets, the Sun, and the Earth's liquid core, correspond to this limit. In the laboratory, an analogous system can be constructed with a very rapidly rotating apparatus, in which the centrifugal force plays the role of self-gravitation. The formulation is offered in such a way that both these geophysical systems and laboratory analogues are included as special cases. When the inclination of the outer boundaries relative to the equatorial plane is considered weak, the two types of system are identical at leading order. In this limit, the asymptotic analysis is profoundly simplified, because the system satisfies the Taylor–Proudman theorem to leading order. Nevertheless the system contains a very peculiar property: the mode defined by a conventional WKBJ theory implicitly assuming a locality of convection in the radial direction perpendicular to the axis of rotation cannot be accepted as a correct marginal mode, because a modulation equation gives an exponential growth in the radial direction, which contradicts an implicit initial assumption. The erroneous behaviour is traced to a spatial dispersion of thermal Rossby waves, which governs the marginal mode. The difficulty is resolved by extending the analysis to a complex plane of the radial coordinate of the point where convection amplitude attains its maximum. Such a complex radial distance is defined as the point where the wave dispersion disappears locally. The projection of the solution onto the real axis results in an inclination of the Taylor columns with respect to the radial direction. This is in good agreement with the most recent numerical studies. The isolation of convective Taylor columns in the radial direction weakens and the spiralling gets stronger as the Prandtl number decreases, as a result of the need to displace the critical radial distance further from the real axis.

1. Introduction

Knowledge of the general behaviour of thermal convection in rapidly rotating systems is crucial to understand various geophysical and astrophysical flows; the fluid motions inside the major planets, the Sun, and the Earth's core are examples. The spherical configuration and self-gravitation are the common features for these systems. A standard formulation of the problem has been given by Chandrasekahr (1961), and an asymptotic linear analysis for the limit of rapid rotation has been developed by Roberts (1968) and Busse (1970). A schematic view of marginal convection inferred from these asymptotic analyses is given in figure 1 of Busse (1970): convection is expected to take the form of an ensemble of Taylor columns

† Current affiliation: NCAR, PO Box 3000, Boulder, Colorado 80307-3000, USA.

aligned along a cylindrical surface coaxial to the axis of rotation. However, the actual radial dependence of the marginal mode is not included in their analysis. An attempt to define the radial dependence of marginal convection in this asymptotic limit is made by Soward (1977). It turns out that within the framework of the previous asymptotic treatment it is not possible to define the radial structure of convection in a consistent manner. The result implies that Roberts' and Busse's analysis does not offer a correct critical Rayleigh number of the system at leading order. The problem has been left untouched since then. The purpose of this paper is to offer a correct critical Rayleigh number of the spherical self-gravitating system, by resolving this difficulty, and hence define the radial structure of the critical mode in a consistent manner.

The problem is worth revisiting at this time, particularly in the light of the recent numerical results by Zhang & Busse (1987) and Zhang (1992). They imply that the morphology of marginal convection at very high rotation rates are qualitatively different from the sketch given by figure 1 in Busse (1970). Two distinctive modes are identified by them: the spiralling and the wall-attached modes. In the spiralling mode, the Taylor columns seem not so strongly constrained to a thin cylindrical shell as expected from the previous asymptotic theory. On the other hand, in the wall-attached mode, the Taylor columns tend to attach to the equatorial boundary, against the expectation from the asymptotic theory that they will reside at an intermediate distance from the axis of rotation. A revised asymptotic theory is required to explain all these discrepancies from the previous theory.

The significance of this problem in a general context of instability theories is equally noted. The difficulty in defining a precise critical Rayleigh number pointed out by Soward is not peculiar to this particular instability problem. Soward & Jones (1983) have encountered and solved a similar difficulty in a spherical Taylor instability problem. A common difficulty can be traced to the interrelations of the global/local temporal/spatial instabilities. Even though much progress has been made for open systems in recent years (e.g. Huerre & Monkewitz 1990), a general analysis for closed systems like the present one is still awaited.

For this reason, an effort is made to keep some generality of the problem in the present study. In this respect, it is worth noting that laboratory analogues of these geophysical systems have been constructed by Busse & Carrigan (1976), Carrigan & Busse (1983). The centrifugal force acting outward from the axis of rotation plays the role of the gravity in these analogues. The correspondence between the geophysical self-gravitating systems and the laboratory systems driven by centrifugal force is first mentioned by Busse (1970). Though the geophysical spherical systems and the laboratory analogue systems are not completely identical, with a simple rescaling of the systems it is believed that the latter provide a good representation of the actual geophysical systems.

In the present paper, a systematic approach unifies these two types of the systems by combining the previous works on both the geophysical systems (e.g. Roberts 1968; Soward 1977; Busse 1983) and the laboratory analogues (e.g. Busse & Hood 1982; Busse 1986). In the next section, the formulation is constructed in such a way that in particular parameter settings both the self-gravitating geophysical systems and the centrifugal-force-driven laboratory systems are recovered. Any intermediate systems can be described in the basic formulation presented in the next section, as long as the symmetry of the outer boundary in respect to the equatorial plane is preserved. A side product of this generality is that we can observe the general nature of the temporal/spatial instabilities in this type of system.

Further, the self-gravitating geophysical systems and their laboratory analogues become asymptotically identical in a limit of weak inclination of the outer boundaries relative to the equatorial plane. In this way a close relationship between two systems is established in a formal manner. Moreover, it is shown that, in this limit, the system can be integrated along the direction of the axis of rotation. Hence, the problem is much simplified in this limit. Because of this simplification, the difficulty pointed out by Soward can be more easily isolated from other factors. It is also shown that the difficulty is inherent to this type of the system, as long as the outer boundaries contain a non-vanishing curvature. The approximation of weak boundary inclinations is introduced in §3, and the analysis is restricted to this limit thereafter. On the other hand, in presenting the numerical results, we focus attention on the case with spherical geometry.

The limit of a weakly inclined boundary is obviously not rigorously justified for the spherical system. We accept this approximation as an essential procedure to simplify the problem to a tractable level. It has been demonstrated by Busse (1970) that this approximation gives results which are in good quantitative agreement with those of a full spherical problem in terms of the previous asymptotic theory. The anticipation is that even in the present revised asymptotic analysis this approximation will be still valid. The comparison of the results with the numerical results for the full spherical system offered in §7 will partly justify the present approximation. Further, a higher-order analysis in Appendix A of the effects of the inclination of the outer boundaries implies asymptotic validity of the approximation. It should be also emphasized that the physical understanding of the marginal modes is improved remarkably by this revision, as elaborated in §8, by resolving the inconsistency of the previous analysis, even though the present results may be valid only in qualitative terms.

The remaining part of this paper is organized as follows. The previous asymptotic analysis by Busse (1970) is reviewed in §4, and the difficulty pointed out by Soward (1977) is explained in §5. An alternative approach to resolve the difficulty is developed in §6, which constitutes a main contribution of the present paper. A special mode which appears in the limit of small Prandtl number is considered in Appendix C.

2. Formulation

In the present work, we adopt the cylindrical coordinate system (s, φ, z), where s represents the distance from the axis of rotation, which is in the z-direction. We adopt the Boussinesq approximation with the coefficient of thermal expansion α to explore the behaviour of thermal convection in a fluid with kinematic viscosity ν and thermal diffusivity κ. The fluid is rotating with angular velocity Ω about the z-axis.

As a basic state, we assume a gravity field

$$\boldsymbol{g} = -g\boldsymbol{r}^{\dagger}/r_0, \tag{2.1a}$$

whose magnitude is measured by a constant g, and a basic temperature distribution

$$\bar{\theta} = \theta_0 - \tfrac{1}{2}\beta \boldsymbol{r}^{\dagger} \cdot \boldsymbol{r}^{\dagger} \tag{2.1b}$$

defined in terms of a constant β, where the vector $\boldsymbol{r}^{\dagger}$ is defined by

$$\boldsymbol{r}^{\dagger} = s\hat{\boldsymbol{s}} + \lambda z \hat{\boldsymbol{z}}, \tag{2.1c}$$

and λ is a free parameter of the problem; r_0 represents the radius of an astronomical body, or a representative size of the laboratory apparatus. With $\lambda = 1$, the system

reduces to a self-gravitating astronomical body, which contains a homogeneous heat source distribution, and with $\lambda = 0$ the system principally† reduces to the laboratory system, in which the gravitational force is mimicked by the centrifugal force. By varying this free parameter, we can easily consider any intermediate situations (though not physically constructable).

After non-dimensionalizing the system by adopting Ωr_0 as the scale of the velocity $\boldsymbol{v}$, βr_0^2 for the perturbation temperature θ, r_0 as the spatial scale, and Ω^{-1} as the time scale, we obtain the non-dimensional perturbation equations

$$(\partial/\partial t - E\nabla^2)\,\boldsymbol{v} + 2\hat{\boldsymbol{k}} \times \boldsymbol{v} = -\nabla\pi + \hat{R}\theta \boldsymbol{r}^{\dagger}, \tag{2.2a}$$

$$\nabla \cdot \boldsymbol{v} = 0, \quad (\partial/\partial t - (E/P)\,\nabla^2)\,\theta - \boldsymbol{v}\cdot\boldsymbol{r}^{\dagger} = 0, \tag{2.2b,c}$$

where

$$\hat{R} = \alpha g \beta r_0/\Omega^2, \quad E = \nu/\Omega r_0^2, \quad P = \nu/\kappa \tag{2.3a–c}$$

are the Rayleigh number, the Ekman number, and the Prandtl number, respectively; $\hat{\boldsymbol{k}}$ is the unit vector in the z-direction.

By introducing the scalar variables ψ and ϕ, any velocity field satisfying the continuity equation (2.2b) is represented by

$$\boldsymbol{v} = \nabla \times \hat{\boldsymbol{k}}\psi + \nabla \times \nabla \times \hat{\boldsymbol{k}}\phi. \tag{2.4}$$

By operation with $\hat{\boldsymbol{k}}\cdot\nabla\times$ and $\hat{\boldsymbol{k}}\cdot\nabla\times\nabla\times$ on (2.2a), we obtain

$$\left(\frac{\partial}{\partial t} - E\nabla^2\right)\Delta_2\psi - 2\frac{\partial}{\partial z}\Delta_2\phi - \hat{R}\frac{\partial\theta}{\partial\varphi} = 0, \tag{2.5a}$$

$$\left(\frac{\partial}{\partial t} - E\nabla^2\right)\nabla^2\Delta_2\phi + 2\frac{\partial}{\partial z}\Delta_2\psi + \hat{R}\left[\lambda z\Delta_2\theta - \left(s\frac{\partial^2}{\partial s\,\partial z} + (1+\lambda)\frac{\partial}{\partial z}\right)\theta\right] = 0, \tag{2.5b}$$

where

$$\Delta_2 \equiv \nabla^2 - (\hat{\boldsymbol{k}}\cdot\nabla)^2.$$

Equation (2.2c) is rewritten as

$$\left(\frac{\partial}{\partial t} - \frac{E}{P}\nabla^2\right)\theta - \left(\frac{\partial\psi}{\partial\varphi} + s\frac{\partial^2\phi}{\partial s\,\partial z}\right) + \lambda z\Delta_2\phi = 0. \tag{2.5c}$$

Equations (2.5a–c) constitute the basic set of equations in the following analysis.

As the boundary condition, we assume that the normal component of the velocity vanishes, i.e.

$$\Delta_2\phi \pm \sigma\frac{\mathrm{d}\eta_{\mathrm{b}}}{\mathrm{d}s}\left(\frac{1}{s}\frac{\partial\psi}{\partial\varphi} + \frac{\partial^2\phi}{\partial s\,\partial z}\right) = 0 \tag{2.6a}$$

at the boundary $z = \pm\eta_{\mathrm{b}}(s)$. In particular, when we assume a spherical configuration of the system, $\eta_{\mathrm{b}}(s)$ is given by

$$\eta_{\mathrm{b}}(s) = (1-s^2)^{\frac{1}{2}}. \tag{2.6b}$$

We have introduced σ as a possible *formal* perturbation parameter, where in the final result we have to set $\sigma = 1$. The perturbation approach is justified when the inclination of the boundary is small enough (i.e. $|\mathrm{d}\eta_{\mathrm{b}}/\mathrm{d}s| \ll 1$).

We restrict our attention to the limit of small Ekman number (i.e. the very rapidly rotating limit) throughout the analysis. Since the equation reduces to the second-order differential equation in this limit in the z-direction, we do not need to consider

† Note that a slightly different basic temperature field is assumed for the laboratory systems. Nevertheless, the final form of the equations obtained below (see (3.1c) and (3.2)) is identical to that obtained for the rotating cylindrical annulus by Busse (1986).

any boundary conditions other than the higher-order corrections due to the boundary layers. The latter effects will be systematically neglected in the analysis, because of its smallness compared to the terms of concern.

The basic strategy of the present study is that, in order to obtain the maximum insight into the system, we retain the generality as much as possible. For this reason, besides the Ekman number E, both the Prandtl number P and σ are dealt with as possible small parameters. From a simple scaling analysis, it is found that the analysis is simplified by the rescalings

$$\hat{R} = \frac{4\epsilon^2\sigma^{\frac{4}{3}}PR}{(1+P)^2}, \quad \hat{m} = \frac{\sigma^{\frac{1}{3}}m}{\epsilon}, \quad \hat{\omega} = \frac{2\sigma\omega}{\hat{m}(1+P)}, \quad \Delta_2 = \hat{m}^2\Delta^*, \tag{2.7a–d}$$

and

$$\epsilon \equiv (E(1+P)/2P)^{\frac{1}{3}}, \tag{2.7e}$$

and $\hat{m}$ and $\hat{\omega}$ represent the non-rescaled azimuthal wavenumber and frequency, respectively. Accordingly, we rescale the dependent variables in terms of E, P, σ by

$$\Delta_2\phi = -\sigma W(s,z)\exp(\mathrm{i}\hat{\omega}t + \mathrm{i}\hat{m}\varphi), \tag{2.8a}$$

$$\mathrm{i}\hat{m}\psi = V(s,z)\exp(\mathrm{i}\hat{\omega}t + \mathrm{i}\hat{m}\varphi), \tag{2.8b}$$

$$2\theta\epsilon\sigma^{\frac{2}{3}} = (1+P)\,\Theta(s,z)\exp(\mathrm{i}\hat{\omega}t + \mathrm{i}\hat{m}\varphi). \tag{2.8c}$$

Consequently, (2.5*a–c*) are reduced to

$$(\omega + \mathrm{i}m^3P\Delta^*)\Delta^*V + (1+P)\frac{\partial W}{\partial z} - \mathrm{i}mPR\Theta = -\frac{\mathrm{i}\epsilon^2mP}{\sigma^{\frac{2}{3}}}\frac{\partial^2}{\partial z^2}\Delta^*V, \tag{2.9a}$$

$$\begin{aligned}\frac{1+P}{\sigma^2}\frac{\partial}{\partial z}\Delta^*V + (\omega + \mathrm{i}m^3P\Delta^*)\Delta^*W + \frac{\mathrm{i}m}{\sigma}PR\lambda^z\Delta^*\Theta \\ = -\left[\frac{\mathrm{i}m\epsilon^2}{\sigma^{\frac{2}{3}}}P\Delta^*\frac{\partial^2}{\partial z^2} + \frac{\epsilon^2}{\sigma^{\frac{2}{3}}}\frac{1}{m^2}(\omega + \mathrm{i}m^3P\Delta^*) + \frac{\mathrm{i}\epsilon^4}{\sigma^{\frac{4}{3}}}\frac{P}{m}\frac{\partial^4}{\partial z^4}\right]W \\ -\frac{\mathrm{i}\epsilon^2}{\sigma^{\frac{5}{3}}}\left(\frac{PR}{m}\right)\left[s\frac{\partial^2}{\partial s\,\partial z} + (1+\lambda)\frac{\partial}{\partial z}\right]\Theta,\end{aligned} \tag{2.9b}$$

$$(\mathrm{i}\omega - m^3\Delta^*)\Theta - m(V + \sigma\lambda zW) = \frac{\epsilon^2m}{\sigma^{\frac{2}{3}}}\frac{\partial^2}{\partial z^2}\Theta - \frac{\sigma^{\frac{1}{3}}\epsilon^2}{m}s\frac{\partial^2}{\partial s\,\partial z}\Delta^{*-1}W, \tag{2.9c}$$

with the boundary condition

$$W \mp \left(\frac{1}{s}\frac{\mathrm{d}\eta_{\mathrm{b}}}{\mathrm{d}s}\right)V \pm \frac{\sigma^{\frac{1}{3}}\epsilon^2}{m}\frac{\mathrm{d}\eta_{\mathrm{b}}}{\mathrm{d}s}\frac{\partial^2}{\partial s\,\partial z}\Delta^{*-1}W = 0 \quad \text{at} \quad z = \pm\eta_{\mathrm{b}}(s). \tag{2.10}$$

The rescalings are a modified version of those found in Soward (1977) and Busse (1983), based on the result of Busse (1970). Asymptotics in the limit of large Prandtl number are taken into account in this version. Also the asymptotics with the small factor σ of the inclination are explicitly represented, so that the gaps between the asymptotic theories for the self-gravitating systems by Roberts (1968) and the laboratory annulus by Busse (1986) are filled. Consequently, the new parameters R, m, ω, the operator Δ^*, and the variables W, V, Θ are expected to be scaled to the order of unity in terms of ϵ, P, and σ, as long as previously estimated asymptotics (Roberts 1968; Busse 1970) are correct. Note that the parameter ϵ mainly measures the magnitude of Ekman number E in the following.

The terms of higher order than $O(\epsilon^2)$ will be neglected in the following analysis. We also restrict our attention to the case where σ is taken as a perturbation parameter, because it is the simplest case of the problem, and still contains the basic features of the problem encountered in the general case. Consequently, a formal ordering assumed in the present paper is $1 \gg \sigma \gg \epsilon$.

3. The limit of small inclination of the boundary

The mathematical treatment of the problem is much simplified in the limit of a small inclination (i.e. $|\mathrm{d}\eta_\mathrm{b}/\mathrm{d}s| \ll 1$). This limit is formally dealt with by taking the parameter σ as a perturbation. Because of the Taylor–Proudman constraint the velocity component in the direction of this axis of rotation can be neglected at the leading order. By assuming this limit, we will return to the spherical geometry (2.6*b*) to obtain the final results in the following. Though the limit of a small inclination of the boundary ($\sigma \ll 1$) is not rigorously justified for the spherical geometry, qualitatively good results are anticipated in this limit, as the previous analysis by Busse (1970) suggests. A justification of this approximation will be obtained by comparing the final results with the numerical results (§ 7).

At leading order in σ, (2.9) reduce to

$$(\omega + \mathrm{i}m^3 P\Delta^*)\,\Delta^* V + (1+P)\,\partial/\partial z\, W - \mathrm{i}mPR\Theta = 0, \tag{3.1a}$$

$$(\partial/\partial z)\,\Delta^* V = 0, \tag{3.1b}$$

$$(\omega + \mathrm{i}m^3\,\Delta^*)\,\Theta + \mathrm{i}mV = 0. \tag{3.1c}$$

Equation (3.1*b*) is a statement of the Taylor–Proudman theorem that the radial component V of velocity is independent of z. Equation (3.1*c*) further implies that Θ is also independent of z. Note that the free parameter λ does not enter into this leading-order system. This means that the gravity force parallel to the direction of the axis of rotation does not enter the dynamics at the leading order, and hence, the equivalence between the cylindrical laboratory system and the self-gravitating spherical system is guaranteed within this approximation. The first-order finite effect of σ is considered in Appendix A.

By integrating (3.1*a*) in the z-direction from $-\eta_\mathrm{b}$ to η_b, we obtain

$$2\eta_\mathrm{b}(\omega + \mathrm{i}m^3 P\Delta^*)\,\Delta^* V + (1+P)\,W|_{z=-\eta_\mathrm{b}}^{\eta_\mathrm{b}} - 2\mathrm{i}mPR\eta_\mathrm{b}\,\Theta = 0.$$

Using the boundary condition (2.10) on the second term, we obtain the final expression

$$[(\omega + \mathrm{i}m^3 P\Delta^*)\,\Delta^* + (1+P)\eta^*]\,V - \mathrm{i}mPR\Theta = 0, \tag{3.2}$$

where

$$\eta^* \equiv (1/s\eta_\mathrm{b})\,\mathrm{d}\eta_\mathrm{b}/\mathrm{d}s \tag{3.3}$$

measures a strength of the *inclination* of the top and bottom boundaries $z = \pm\eta_\mathrm{b}(s)$, and can also be considered as a generalized *topographic* beta effect (e.g. Pedlosky 1987; see also Ingersoll & Pollard 1982) of the system. Equations (3.1*c*) and (3.2) constitute a complete problem, along with the appropriate boundary conditions in the s-direction. Note the similarity (3.2) to the quasi-geostrophic equivalent barotropic system, apart from the last term due to the buoyancy force.

The problem is stated, in more formal terms, as

$$\mathrm{L}_{11}\,V + \mathrm{L}_{12}\,\Theta = 0, \quad \mathrm{L}_{21}\,V + \mathrm{L}_{22}\,\Theta = 0, \tag{3.4a,b}$$

where
$$\mathrm{L}_{11} = [(\omega + \mathrm{i}m^3 P\Delta^*)\Delta^* + (1+P)\eta^*], \tag{3.5a}$$
$$\mathrm{L}_{12} = -\mathrm{i}mPR, \quad \mathrm{L}_{21} = \mathrm{i}m, \quad \mathrm{L}_{22} = \omega + \mathrm{i}m^3\Delta^*. \tag{3.5b–d}$$

By setting
$$V = \mathrm{L}_{22}\Phi, \quad \Theta = -\mathrm{L}_{21}\Phi, \tag{3.6}$$

the problem is reduced to
$$\mathscr{L}(m, \Delta^*, \omega, R, \eta^*)\Phi = 0, \tag{3.7}$$

where
$$\mathscr{L}(m, \Delta^*, \omega, R, \eta^*) \equiv \hat{\mathscr{L}}(m, \Delta^*, \omega, \eta^*) - m^2 PR, \tag{3.8a}$$

and
$$\hat{\mathscr{L}}(m, \Delta^*, \omega, \eta^*) \equiv [(\omega + \mathrm{i}m^3 P\Delta^*)\Delta^* + (1+P)\eta^*](\omega + \mathrm{i}m^3\Delta^*). \tag{3.8b}$$

Note that the operator $\mathscr{L}$ has been defined as the determinant of the operator matrix $\mathbf{L}$:
$$\mathscr{L} \equiv \mathrm{L}_{11}\mathrm{L}_{22} - \mathrm{L}_{12}\mathrm{L}_{21}$$
in the current cylindrical problem. The corresponding operator $\mathscr{L}$ in the full spherical problem (with $\sigma \sim O(1)$) can also be defined in an analogous way: the determinant of the operator matrix $\mathbf{L}$, but in this case defined in terms of a solvability condition for the dependence, instead of a simple matrix determinant. For this reason, it is understood that the cylindrical problem and the full spherical problem have basically the same mathematical structure, and the former acts as a simplified version of the latter, containing essentially the same feature of the problem. The analysis on the finite effect of σ in Appendix A implies that the leading-order problem in the σ-expansion is equivalent to taking the leading component of Taylor expansions in the z-direction of the full problem. In the full spherical problem, an equivalent process is performed to obtain (3.2) from (3.1a) by the z-integration of (3.1a) multiplied by the eigenmode of V in the z-direction.

4. Leading-order analysis: conventional approach

The leading-order problem of the system (3.1c) and (3.2) has been considered by Busse (1970), as a laboratory analogue of the full spherical problem. However, we encounter a difficulty even with this version of the problem, as in the case of the full spherical problem, which has been pointed out by Soward (1977). It will be considered in the next section and a solution to the difficulty will be addressed in §6. We first review the analysis of Busse (1970) in this section.

We assume a WKBJ-type plane wave solution
$$\Delta^* = -\alpha^2 \equiv -(1/s_0^2 + k^2/m^2)$$
localized at $s = s_0$, where k is the radial wavenumber, normalized in the same manner as the azimuthal wavenumber m. The anticipation is that we will obtain a localized wave envelope as a modulation of the leading order WKBJ solution at a higher order. By replacing all the s-dependent variables by the values at $s = s_0$, (3.7) reduces to an algebraic equation
$$R(m, -\alpha^2, \omega, \eta_0^*) = (1/m^2 P)\,\hat{\mathscr{L}}(m, -\alpha^2, \omega, \eta_0^*), \tag{4.1a}$$

where
$$\eta_0^* \equiv \eta^*(s = s_0).$$

The assumption of a real Rayleigh number R defines the frequency by
$$\omega = \eta_0^*/\alpha^2. \tag{4.1b}$$

The variation of (4.1a) gives
$$\delta R/R_\omega = (R_m/R_\omega)\,\delta m + (R_k/R_\omega)\,\delta k + (R_{s_0}/R_\omega)\,\delta s_0 + \delta\omega.$$

Here the partial differentiations are done by keeping all the other quantities, m, k, s_0, and ω, fixed. Note that α is considered as a dependent variable of both k and s_0, and η_0^* is a dependent variable of s_0. The variation is made under the constraint of real Rayleigh number, which is accomplished by substituting the dispersion relation (4.1b) into the variations to obtain the final result. Note that, despite this constraint, the differentiations to define the variations are done by pretending that, nevertheless, ω is an independent variable. At the critical point, the variation δR vanishes for any arbitrary infinitesimal real variations of wavenumbers m, k and the position s_0 by appropriately variating the frequency ω along the real axis in accordance with the dispersion relation (4.1b). This requirement is equivalent stated by

$$\mathrm{Im}\,[R_m/R_\omega]=0, \quad \mathrm{Im}\,[R_k/R_\omega]=0, \quad \mathrm{Im}\,[R_{s_0}/R_\omega]=0, \tag{4.2a–c}$$

where

$$R_\omega=\frac{1}{m^2P}\frac{\partial\hat{\mathscr{L}}}{\partial\omega}, \quad R_m=-\frac{2}{m^3P}\hat{\mathscr{L}}+\frac{1}{m^2P}\frac{\partial\mathscr{L}}{\partial m}, \tag{4.3a,b}$$

$$R_k=\frac{1}{m^2P}\frac{\partial\hat{\mathscr{L}}}{\partial\alpha^2}\frac{\partial\alpha^2}{\partial k}\equiv\frac{1}{m^2P}\mathrm{i}\frac{\partial\hat{\mathscr{L}}}{\partial(\partial/\partial s)}, \tag{4.3c}$$

$$R_{s_0}=\frac{1}{m^2P}\left(\frac{\partial\hat{\mathscr{L}}}{\partial\alpha^2}\frac{\partial\alpha^2}{\partial s_0}+\frac{\partial\hat{\mathscr{L}}}{\partial\eta_0^*}\frac{\mathrm{d}\eta_0^*}{\mathrm{d}s_0}\right)\equiv\frac{1}{m^2P}\left(\frac{\partial\hat{\mathscr{L}}}{\partial s_0}\right). \tag{4.3d}$$

After some manipulations, the conditions (4.2a–c) lead to

$$m^6\alpha^8-\tfrac{1}{2}\eta_0^{*2}=0, \quad kP(\eta_0^{*2}-3m^6\alpha^8)=0, \quad \eta_0^*-2s_0\,\mathrm{d}\eta_0^*/\mathrm{d}s_0=0, \tag{4.4a–c}$$

where the dispersion relation (4.1b) has been used in the final expressions.

The condition (4.4a) gives a critical azimuthal wavenumber m, and the critical radial wavenumber k defined from (4.4b), consistent with (4.4a), is $k=0$. It means that the radial wavenumber k is much smaller than the azimuthal wavenumber m, and, consequently, the radial dependence of convection is to be determined at a higher order. Note that the position of convection is defined by the curvature $\mathrm{d}\eta^*/\mathrm{d}s_0$ of the boundary, in general. When we assume the spherical geometry defined by (2.6b) or

$$\eta^*=-1/(1-s^2), \tag{4.5}$$

the position of convection is given by $s_0=1/\sqrt{5}=0.447\ldots$ from (4.4c). Accordingly, the other critical parameters are given by

$$\eta^*=-1.25, \quad \omega=-0.25, \quad m=0.328\ldots, \quad R=4.351\ldots\equiv R_0. \tag{4.6a–d}$$

The analysis to a higher order in σ given in Appendix A shows that the critical Rayleigh number is corrected to

$$R=(1+\tfrac{2}{3}\sigma\lambda)R_0 \tag{4.7}$$

at $O(\sigma)$. Consequently, for the full spherical self-gravitating system ($\sigma=1$, $\lambda=1$), a precise critical Rayleigh number is given by multiplying by the factor $\frac{5}{3}$ the leading-order value R_0. A systematic discrepancy between the critical Rayleigh numbers evaluated analytically as in the present section and those evaluated with a numerical approach, represented in figure 2 of Busse (1970), is explained by this term. Note that the correction formula (4.7) is independent of the specific approach adopted to evaluate the leading-order critical values. Hence, the correction formula (4.7) can also be applied to the result obtained by a revised version of the asymptotic theory in §6.

5. The radial dependence consistent with the conventional approach

The analysis of the previous section implies that the radial dependence of convection is still small (say of order $\hat{\epsilon}$), but much longer than the scale of the azimuthal direction (i.e. $\epsilon \ll \hat{\epsilon}$). As explained at the beginning of the previous section, it is expected that such a radial dependence is defined in terms of a wave modulation equation. (Note that, in the present case, the wave to be modulated has no wavenumber. Nevertheless, this does not invalidate the multiple-scale method.) For this purpose, we introduce the following rescaling of the radial direction:

$$\partial/\partial s = \hat{\epsilon}^{-1}\partial/\partial\xi, \quad s = s_0 + \hat{\epsilon}\xi. \tag{5.1}$$

Subsequently, it is found that the Laplacian is written

$$\Delta^* = -\frac{1}{s_0^2} + \hat{\epsilon}\left(\frac{2}{s_0^3}\xi + \frac{1}{m^2}\frac{\partial^2}{\partial\xi^2}\right) \tag{5.2}$$

with $$\hat{\epsilon} \equiv \epsilon^{\frac{3}{5}}/\sigma^{\frac{3}{5}}.$$

By substitution of (5.2) and by Taylor expanding the boundary inclination η^* around $s = s_0$, we obtain an equation of order $\hat{\epsilon}$ from (3.7). Equivalently, more formally, the equation to define the radial dependence is written, as a wave modulation equation (e.g. Kawahara 1973), by

$$\left[\frac{1}{2}\frac{\partial^2\hat{\mathscr{L}}}{\partial(\partial/\partial s)^2}\frac{\partial^2}{\partial\xi^2} + \frac{\partial\hat{\mathscr{L}}}{\partial s_0}\xi + \frac{\partial\hat{\mathscr{L}}}{\partial\omega}\omega_1 - m^2PR_1\right]\Phi = 0, \tag{5.3}$$

where

$$\frac{1}{2}\frac{\partial^2\hat{\mathscr{L}}}{\partial(\partial/\partial s)^2} \equiv -\frac{1}{m^2}\frac{\partial\hat{\mathscr{L}}}{\partial\alpha^2} = \frac{1}{m^2}\left[\omega^2 - \frac{3m^6P}{s_0^4} - \mathrm{i}m^3(1+P)\frac{\omega}{s_0^2}\right], \tag{5.4a}$$

$$\frac{\partial\hat{\mathscr{L}}}{\partial s_0} \equiv \frac{\partial\hat{\mathscr{L}}}{\partial\alpha^2}\frac{\partial\alpha^2}{\partial s_0} + \frac{\partial\hat{\mathscr{L}}}{\partial\eta_0^*}\frac{\mathrm{d}\eta_0^*}{\mathrm{d}s_0} = \frac{2}{s_0^3}\left[\omega^2 - \frac{3m^6P}{s_0^4} - \mathrm{i}m^3(1+P)\frac{\omega}{s_0^2} + (1+P)\omega^2\left(\omega - \frac{\mathrm{i}m^3}{s_0^2}\right)\right], \tag{5.4b}$$

$$\frac{\partial\hat{\mathscr{L}}}{\partial\omega} = -\left(2\omega - \frac{\mathrm{i}m^3}{s_0^2}P\right)\frac{1}{s_0^2} + (1+P)\frac{\omega}{s_0^2}, \tag{5.4c}$$

and ω_1 and R_1 are the correction to the frequency and the critical Rayleigh number at $O(\hat{\epsilon})$. Note that in the final expression (5.4), the form (4.5) of the boundary has been assumed. The solution of (5.3) is written in terms of an Airy function as

$$\Phi(\xi) = \mathrm{Ai}\,(\mu(\xi + \xi_0)), \tag{5.5}$$

where

$$\mu^3 = -\frac{\partial\hat{\mathscr{L}}}{\partial s_0}\Big/\frac{1}{2}\frac{\partial^2\hat{\mathscr{L}}}{\partial(\partial/\partial s)^2}, \quad \mu^3\xi_0 = \left(\frac{\partial\hat{\mathscr{L}}}{\partial\omega}\omega_1 - m^2PR_1\right)\Big/\frac{1}{2}\frac{\partial^2\hat{\mathscr{L}}}{\partial(\partial/\partial s)^2}. \tag{5.6a, b}$$

Here, as pointed out by Soward (1977) for the full spherical problem, we encounter a difficulty. The coefficient μ is complex, in general, in the present problem, while the Airy function $\mathrm{Ai}(\zeta)$ grows exponentially as $\zeta \to \infty$ in general for a complex variable ζ. It decays exponentially only in the section $|\mathrm{ph}(\zeta)| < \frac{1}{3}\pi$, and decays algebraically only along the real axis as $\zeta \to -\infty$ (e.g. Olver 1974). Consequently, the asymptotic solution defined in the previous section grows exponentially as $\xi \to +\infty$ in general. ($\mathrm{Re}\,(\mu) < 0$ is proved for every Prandtl number, by assuming (4.5), and $\mathrm{Im}\,(\mu) \neq 0$ apart from the special cases discussed below.) Note that the zeros of the Airy function are distributed only along the real axis (and all negative), so that the solution cannot

be bounded in any sense as $\xi \to +\infty$. In other words, the convection mode inferred at leading order in the previous section is not locally isolated as initially assumed. Hence, the critical point defined in the previous section is not consistent, and for this reason, cannot be a correct critical point. The implication is that the actual critical Rayleigh number has a finite value larger than the one defined by the analysis of the previous section.

An elucidating physical interpretation of this difficulty in terms of wave dispersions is given by Soward (1977), as described briefly in Appendix B, More heuristically, it can be understood that the difficulty stems from the coexistence of temporal and spatial instabilities. An exponentially exploding spatial mode, represented in terms of an Airy function, implies that an initial small disturbance, set up near to $s = s_0$, grows exponentially as it propagates. However, such an exponential blow-up mode cannot be confined to a spherical container. Instead, by repeated reflections at the boundaries, it is finally dispersed by diffusivity. (Note that the perturbation is temporally absolutely stable apart from close to $s = s_0$.) Consequently, even in terms of temporal evolution, the mode supposedly defined as a marginal mode in the previous section cannot be persistent, as long as linear dynamics are concerned. For the role of nonlinearities, refer to Soward (1977).

Note that, when the boundary inclination $\eta^*(s)$ does not depend on the distance s, the difficulty does not arise. In this case, the second term in (5.4a) drops out, hence the coefficient $\partial\hat{\mathscr{L}}/\partial s_0$ is equal to $\partial\hat{\mathscr{L}}/\partial(\partial/\partial s)^2$ apart from a real constant factor $\partial\alpha^2/\partial s_0$. It is seen that the curvature of the boundary, which defines a dispersion relationship of the linear waves, is a crucial part of the difficulty (Appendix B).

The other exceptional case is the limit of small Prandtl number. It is seen that, in this limit, the coefficient μ tends to reality, and, hence, a consistent solution is available. In this respect, a separate analysis of this limit should be done. Since the Prandtl number measures the relative magnitude of the kinematic viscosity compared to the thermal diffusivity, it is inferred that the kinematic viscosity is responsible for an erroneous spatial instability of the system. In contrast, in the limit of small Prandtl number, where the viscosity plays no role in the leading order, the motion is described as a pure inertial oscillation (Greenspan 1968). At a higher order, a weak thermal perturbation is required to sustain the motion against weak dissipation by viscosity. A preliminary analysis for this limit is given in Appendix C.

6. An alternative approach

The general nature of the difficulty encountered in the previous section has been elucidated by Soward & Jones (1983). As stated in §4, a general condition for the critical point is given by the set of conditions (4.2a–c). Soward & Jones remark that, in a usual situation, the conditions (4.2b, c) can be replaced by

$$R_k = 0, \quad R_{s_0} = 0. \tag{6.1a, b}$$

In the present problem, though the condition (4.2b) is replaceable with (6.1a), the condition (4.2c) cannot be replaced by (6.1b), which causes a difficulty. If (6.1b), which leads to $\partial\hat{\mathscr{L}}/\partial s_0 = 0$ from (4.3d), is satisfied, the term proportional to ξ in (5.3) does not appear in the problem. Instead, higher-order derivatives of the operator $\hat{\mathscr{L}}$ are considered, namely

$$\left[\frac{1}{2}\frac{\partial^2\hat{\mathscr{L}}}{\partial(\partial/\partial s)^2}\frac{\partial^2}{\partial\xi^2} + \frac{\partial^2\hat{\mathscr{L}}}{\partial(\partial/\partial s)\,\partial s_0}\xi\frac{\partial}{\partial\xi} + \frac{1}{2}\frac{\partial^2\hat{\mathscr{L}}}{\partial s_0^2}\xi^2 + \frac{\partial\hat{\mathscr{L}}}{\partial\omega}\omega_1 - m^2PR_1 + \mathscr{B}\right]\Phi = 0, \tag{6.2a}$$

with $$\hat{\epsilon} \equiv \epsilon^{\frac{1}{4}}/\sigma^{\frac{1}{4}},$$

and an additional constant $\mathscr{B}$ expected from a permutation of operators $\xi\partial/\partial\xi$ and $(\partial/\partial\xi)\xi$ based on a boundary condition; in the present problem, it is fortunate that $\partial^2\mathscr{L}/[\partial(\partial/\partial s)\,\partial s_0] = 0$ and hence $\mathscr{B} = 0$.

By reducing the turning point $s = s_0$ from the first order to the second order in (6.2*a*), we can cast the solution into the form of a Weber function

$$\Phi = \exp(\mathrm{i}\omega_1 t - \xi^2/2\gamma)\, H_n(\xi/b), \tag{6.2b}$$

where $$\gamma = \frac{\partial^2\hat{\mathscr{L}}}{\partial(\partial/\partial s)^2}\Big/\left(\frac{\partial^2\hat{\mathscr{L}}}{\partial(\partial/\partial s)\,\partial s_0} + \mathscr{D}\right), \quad b^2 = \frac{\partial^2\hat{\mathscr{L}}}{\partial(\partial/\partial s)^2}\Big/\mathscr{D},$$

and $$\mathscr{D}^2 = -\frac{\partial^2\hat{\mathscr{L}}}{\partial(\partial/\partial s)^2}\frac{\partial^2\hat{\mathscr{L}}}{\partial s_0^2} + \left[\frac{\partial^2\hat{\mathscr{L}}}{\partial(\partial/\partial s)\,\partial s_0}\right]^2.$$

Here the corrections to the frequency ω_1 and Rayleigh number R_1 are related to the integer n by

$$-\frac{\partial\hat{\mathscr{L}}}{\partial\omega}\omega_1 = -m^2 P R_1 - \left[\frac{1}{2}\left(\frac{\partial^2\hat{\mathscr{L}}}{\partial(\partial/\partial s)\,\partial s_0} + \mathscr{D}\right) + n\mathscr{D}\right],$$

and $H_n(x)$ is the nth Hermite polynomial. The sign of the coefficient γ is chosen to be $\mathrm{Re}(\gamma) > 0$, which guarantees the solution (6.2*b*) decays exponentially away from the turning point $s = s_0$, so that the type of difficulty encountered in the present case does not appear.

The difficulty of the present problem stems from the fact that, though the condition (4.2*c*) is satisfied at the critical point, $\mathrm{Re}[R_{s_0}/R_\omega]$ remains non-zero (i.e. (6.1*b*) is not satisfied). Consequently, the modulation equation to define the radial structure reduces to the form (5.3) instead of (6.2). It is easily proved (Appendix B) that we encounter this kind of difficulty whenever the marginal mode contains a spatially dispersive wave. In the present case, Rossby wave dispersion (4.1*b*) causes the difficulty. (Note again that if the effect of viscosity is weak enough (i.e. $P \to 0$), even with the dispersion, (5.3) offers a well-behaved solution.)

A recipe to resolve the difficulty proposed by Soward & Jones (1983) is to replace the condition (4.2*c*) by (6.1*b*).† For this purpose we have to extend the analysis to the complex s_0-plane with $s_0 = s_r + \mathrm{i}s_i$. Now s_0 is a complex distance from the axis of rotation, where the centre of convection is situated. On the complex s_0-plane, we seek the point where the condition (6.1*b*) is completely satisfied, along with the other conditions (4.2*a*, *b*). In practice, we proceed in the following way:

The dispersion relation to constrain the variations is defined by the reality of the Rayleigh number as before. By referring to (4.1*a*), it is equivalently stated by

$$\hat{\mathscr{L}}_i = 0, \tag{6.3a}$$

where we have designated the real and imaginary components of the operator $\mathscr{L}(m, -\alpha^2, \omega, \eta_0^*)$ by

$$\hat{\mathscr{L}} = \hat{\mathscr{L}}_r + \mathrm{i}\hat{\mathscr{L}}_i.$$

Equation (6.3*a*) is a second-order algebraic equation in terms of ω. One root, which is continuous to (4.1*b*) on the real axis, is adopted for the analysis. The other root becomes infinite on the real axis. By substituting the expression for ω into the partial differentiations in (4.2*a*, *b*), we define the critical wavenumbers k and m at any given

† An equivalent proposal has been made by Huerre & Monkewitz (1990) for open systems. The condition (4.2*b*) must be also replaced by (6.1*a*) in the general case.

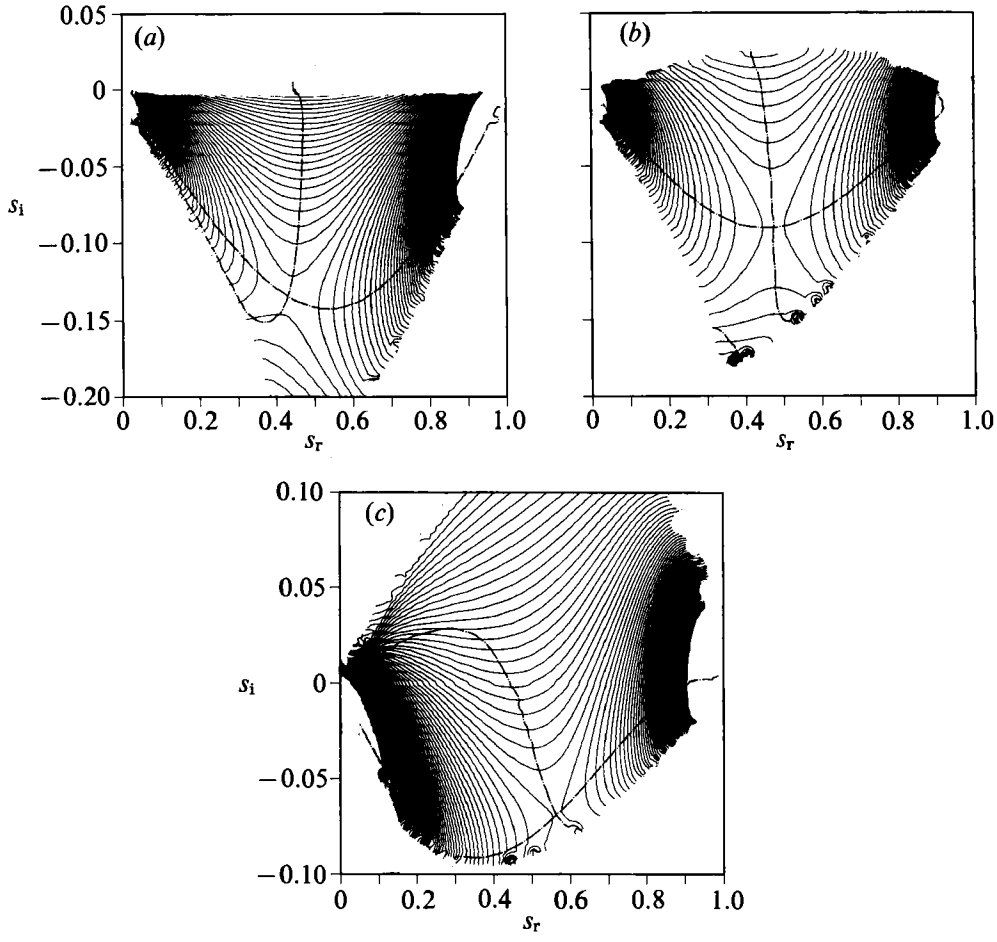

FIGURE 1. The Rayleigh number satisfying the conditions (4.2a, b) plotted on the complex plane $s_0 = s_r + is_i$ for (a) $P = 0.1$, (b) $P = 1$, (c) $P = 10$. The contours are drawn with an interval 0.5 up to 50 in (a), and 0.2 up to 20 in (b, c). The chain-dotted curves are for $\delta R/\delta s_r = 0$ and $\delta R/\delta s_i = 0$. No attempt to plot the Rayleigh number on a whole domain is made, because of the numerical difficulty in tracing the critical value as the survey moves away from the saddle point, in particular due to a dramatic increase of the critical azimuthal wavenumber m.

point on the s_0-plane. The critical radial wavenumber is simply given by $k = 0$ from (4.2b) or (6.1a) as before. Note that the radial wavenumber enters the operator $\hat{\mathscr{L}}$ only in the square form through the Laplacian Δ^*. By referring to (4.3c), equation (4.2b) is equivalent to

$$k \operatorname{Im} [\partial \hat{\mathscr{L}} / \partial \alpha^2 / R_\omega] = 0.$$

The condition $\operatorname{Im} [\partial \hat{\mathscr{L}} / \partial \alpha^2 / R_\omega] = 0$ is not competitive with the condition (4.2a) in general, as in the analysis along the real axis (see (4.4)). Hence the vanishing of the radial wavenumber follows from the condition (4.2b). The same condition follows from (6.1a), too. On the other hand, the critical azimuthal wavenumber m is kept real in order to preserve the homogeneity of the solution in the φ-direction. By choosing the critical m at every given point satisfying the condition (4.2a), we week the point s_0, where the condition (6.1b) is satisfied.

The procedure is visualized in figure 1 (a–c), where we plot the Rayleigh number

$$R = \hat{\mathscr{L}}_r / m^2 P \qquad (6.3b)$$

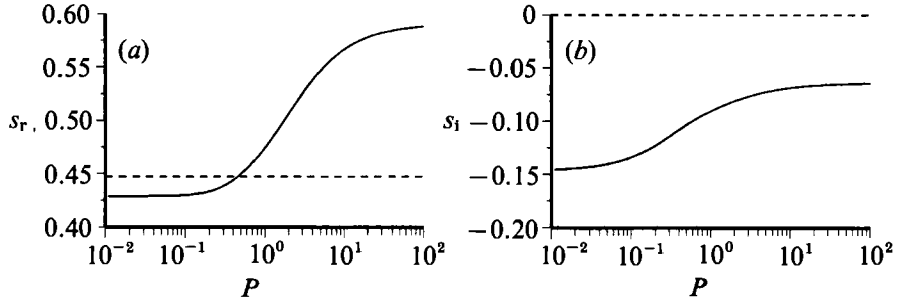

FIGURE 2. The dependence of the saddle point $s_0 = s_r + is_i$ on the Prandtl number P: (a) real component s_r, (b) imaginary component s_i.

with $k = 0$ consistent with (4.2b), m defined by (4.2a), and the frequency ω defined from the dispersion relation (6.3a) on the s_0-plane for $P = 0.1$, 1, 10, respectively. Since the two conditions (4.2a, b) are already satisfied on the plots, it only remains to identify a point, where the condition (6.1b) is satisfied. To help to understand the procedure, the curves of both $\delta R/\delta s_r \equiv \partial R/\partial s_r + \partial R/\partial\omega(\partial\omega/\partial s_r) = 0$ and $\delta R/\delta s_i = 0$ are shown as chain-dotted curves. The critical point defined in §4 by condition (4.2c) is identified as a point with $\delta R/\delta s_r = 0$ along the real axis (Appendix D, §D.1). It is seen that at this point, though a local minimum of Rayleigh number is attained along the real axis, it is not a local extremum in the direction of the imaginary component (i.e. $\delta R/\delta s_i \neq 0$). This dispersive nature of the solution causes a difficulty.

The necessity to depart from the real axis is understood visually on the figures in that there is no point along the real axis where the condition (6.1b), or equivalently $\delta R/\delta s_0 = 0$ (Appendix D, §D.2) is completely satisfied. On the other hand, on leaving the real axis downward on the complex plane, the local minimum of the Rayleigh number increases, along the curve $\delta R/\delta s_r = 0$, until it attains a maximum at the point $\delta R/\delta s_i = 0$, which constitutes a saddle point (Appendix D, §D.3). At this point, where the condition (6.1b) is satisfied, the local asymptotic solution can be cast into an equation of the form (6.2) so that the problem of non-localization is resolved.

Though it may seem physically meaningless to consider a solution localized on a complex plane, formally it simply means that we replace the Laplacian Δ^* in (3.7) by a complex eigenvalue $\alpha^2 \equiv 1/s_0^2$ in (4.1a). An equivalent analysis can also be done in terms of the local complex total wavenumber α, instead. Since we have kept the leading-order wavenumber k vanishing, the saddle point identified also constitutes a turning point, where the wavenumber vanishes locally. Appendix B further tells us that it is also a point where the wave dispersion vanishes locally along the curve $\delta R/\delta s_r = 0$. As a result, we obtain a well-behaved non-dispersive solution (6.2b) near to $s = s_0$. The anticipation is that such a property is preserved globally, so that we still obtain a localized solution along the real axis. We will examine this point below.

Figure 2 represents the dependence of the position s_0 of the saddle point on Prandtl number P. It is seen that a greater shift of the critical point s_0 from the real axis is required for a smaller Prandtl number, so that a larger discrepancy from the conventional asymptotic analysis is expected for this case. The Rayleigh number R and the frequency ω at a defined critical point (the saddle point) s_0 are represented by figures 3(a) and 3(b), respectively, along with the critical azimuthal wavenumber m in figure 3(c).

The radial dependence of the solution is determined from

$$(\hat{\mathscr{L}}(m, \Delta^*, \omega, \eta^*) - \hat{\mathscr{L}}(m, -1/s_0^2, \omega, \eta_0^2))\,\Phi = 0, \tag{6.4}$$

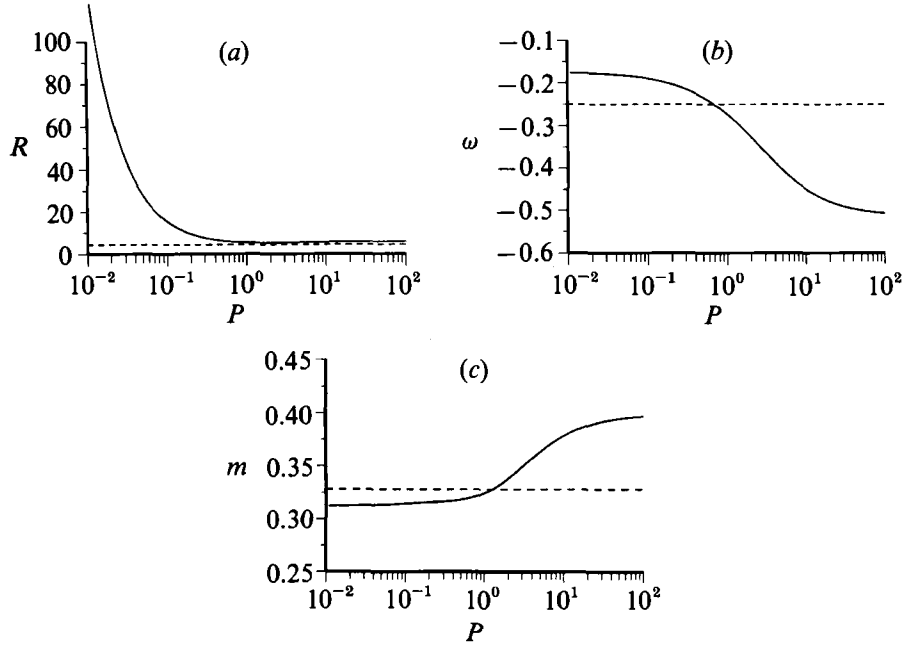

FIGURE 3. The dependence of the critical parameters on the Prandtl number P: (*a*) Rayleigh number R, (*b*) frequency ω, (*c*) azimuthal wavenumber m.

where m, ω, and η_0^* take their values at the saddle point $s = s_0$. The expression is equivalent to (3.7) from (4.1a). If we approximate the Laplacian Δ^* by

$$-1/s^2+(1/\hat{m}^2)\,\partial^2/\partial s^2,$$

(6.4) is written

$$\left[\left(\frac{1}{\hat{m}}\right)^6 C_3\frac{\partial^6}{\partial s^6}+\left(\frac{1}{\hat{m}}\right)^4 C_2\frac{\partial^4}{\partial s^4}+\left(\frac{1}{\hat{m}}\right)^2 C_1\frac{\partial^2}{\partial s^2}+C_0\right]\Phi = 0, \tag{6.5}$$

where

$$C_3 \equiv \frac{1}{6}\frac{\partial^3\hat{\mathscr{L}}}{\partial\Delta^{*3}}\bigg|_{\Delta^*=-1/s^2} = -m^6P, \tag{6.6a}$$

$$C_2 \equiv \frac{1}{2}\frac{\partial^2\hat{\mathscr{L}}}{\partial\Delta^{*2}}\bigg|_{\Delta^*=-1/s^2} = im^3\omega(1+P)+\frac{3m^6P}{s^2}, \tag{6.6b}$$

$$C_1 \equiv \frac{\partial\hat{\mathscr{L}}}{\partial\Delta^*}\bigg|_{\Delta^*=-1/s^2} = \omega^2-\frac{3m^6P}{s^4}+im^3(1+P)\left(-\frac{2\omega}{s^2}+\eta^*\right), \tag{6.6c}$$

$$C_0 \equiv \hat{\mathscr{L}}(m,-1/s^2,\omega,\eta^*)-\hat{\mathscr{L}}(m,-1/s_0^2,\omega,\eta_0^*). \tag{6.6d}$$

Consequently, the local radial wavenumber $\hat{k}(s)$ defined by $\partial/\partial s \equiv i\hat{k}$ is determined from the algebraic equation

$$-C_3k^6+C_2k^4-C_1k^2+C_0 = 0,$$

where

$$k = \hat{k}/\hat{m}.$$

(Note that a different normalization is adopted for the radial wavenumber k than that of §4.) It is seen that there are three pairs of roots, each having an opposite sign in both real and imaginary components to the other. Note that with these modified asymptotics the radial wavenumber is of the same order as that of the azimuthal component.

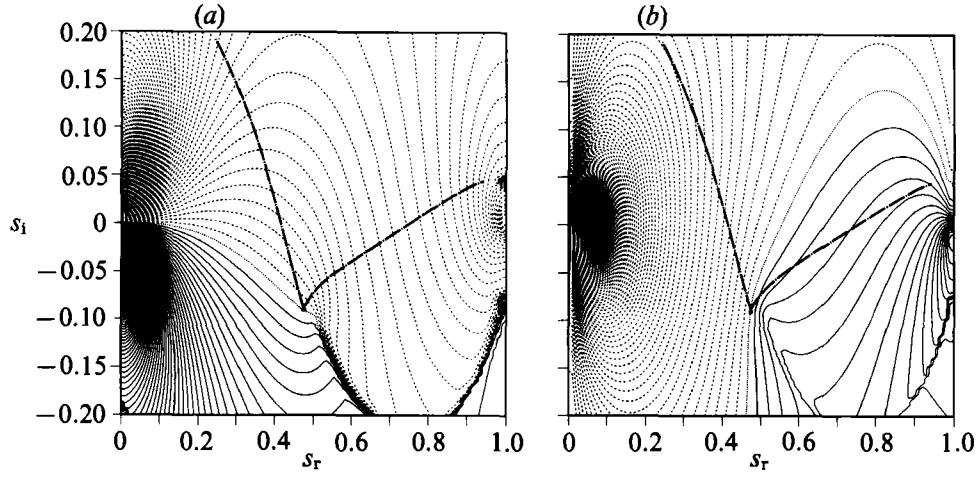

FIGURE 4. The distribution of the complex wavenumber $k = k_r + ik_i$ on the complex plane $s = s_r + is_i$ with $P = 1$: (*a*) the real part k_r, (*b*) the imaginary part k_i. The contour interval is 0.2 from -100 to 100. Negative areas are drawn with dashed curves, while the zero lines are designated by dotted curves. The saddle point s_0 is represented by a black circle. The anti-Stokes lines are drawn from the saddle point by chain-dotted curves.

Among possible pairs of roots we choose a pair $\pm k$ such that the local radial wavenumber vanishes at the saddle point $s = s_0$. The distribution of one of the pairs of roots $k(s) = k_r(s) + ik_i(s)$ on the complex s-plane are shown in figure 4 for the case with $P = 1$. It is seen that the imaginary component $k_i(s)$ of the root changes sign along the real axis. By crossing the point $s = s_t$ with $k_i(s) = 0$ along the real axis, the mode changes from an exponentially growing to an exponentially decaying mode, which allows a localized solution around this point. (Note that another pair $-k(s)$ has an opposite property which offers a non-localized solution around this point.)

The solution is approximately expressed by

$$\Phi \approx \Phi_0 \exp\left[i\hat{k}_r(s_t)(s-s_t) + \left(i\frac{\partial \hat{k}_r(s_t)}{\partial s_r} - \frac{\partial \hat{k}_i(s_t)}{\partial s_r}\right)\frac{(s-s_t)^2}{2}\right] \tag{6.7}$$

around the turning point $s = s_t$ of $k_i(s_r)$. It is seen that the sign of k_i should be chosen in such a way that it satisfies

$$\partial \hat{k}_i(s_t)/\partial s_r > 0$$

in order to obtain a localized solution. The marginal convection has a Gaussian profile peaked at $s = s_t$, with a wave structure, with a constant phase along the direction

$$\hat{m}\varphi + \hat{k}_r(s_t)(s-s_t) = \hat{m}[\varphi + k_r(s_t)(s-s_t)] = \text{const.}$$

around $s = s_t$. Hence, the magnitude of the eastward tilting of the vortex columns with increasing distance s from the axis of rotation is locally defined by

$$\theta \equiv -\tan^{-1} k_r(s_t), \tag{6.8}$$

while the steepness of the Gaussian profile may be measured by $\partial \hat{k}_i/\partial s_r(s_t)$. The dependence of these quantities characterizing the convection columns on Prandtl number is shown in figure 5(*a*, *b*), respectively, along with the position s_t of the turning point in figure 5(*c*).

Finally, a little care should be paid for a consistence for a higher-order correction of WKBJ approximation. Even though we have obtained a solution bounded in both directions of s to leading order, we also bear in mind the other solution of the pair described by a local wavenumber $-k$, which grows exponentially, departing from the turning point s_t in contrast to the leading-order solution. Here, the main eigensolution is *dominant* and the remaining one is *recessive* near $s = s_t$. (Here, dominance and recession have roughly their literal meaning, but see Olver 1974 for a more exact definition.) In general we require two independent *numerically satisfactory* solutions (Olver 1974, Ch. 5; Miller 1950), each dominant in a different range of the domain of concern (in this case $[0, 1]$), respectively, to satisfy the boundary conditions. At a higher order the eigensolution, which has been chosen at a leading order, is not sufficient to satisfy the boundary conditions of the problem at $s = 0, 1$ satisfactorily. For this purpose, we have to add the other eigensolution of the pair as a higher-order correction. A necessary condition to construct a satisfactory solution at a higher order by the combination of two eigensolutions is that the remaining eigensolution is dominant at near the boundaries $s = 0, 1$, so that it can offer an appropriate correction to the leading-order solution, which is recessive in turn near the boundaries, to satisfy the boundary conditions at a higher order.†

For a pair of WKBJ solutions, the dominance of the eigensolutions changes from one pair to the other over the anti-Stokes lines (e.g. Olver 1974) defined by

$$\mathrm{Im}\left[\int_{s_0}^{s} k\,\mathrm{d}s\right] = 0.$$

The anti-Stokes lines are drawn as chain-dotted curves in figure 4 (a, b). Let us define the two points where the anti-Stokes lines cross the real axis as s_1 and $s_2 (s_1 < s_2)$. In the range (s_1, s_2), the primary solution locally described by (6.7) is dominant, while outside the range (s_1, s_2) the remaining one of the pair is dominant. Consequently, the anti-Stokes lines should cross the real axis within the range of the interest (i.e. $0 < s_1 < s_2 < 1$), in order that the system contains two independent numerically satisfactory solutions.

To check the consistency of the WKBJ analysis, the cross points s_1 and s_2 of the anti-Stokes lines are plotted as dashed curves on figure 5 (c). It is seen that the larger crossing point s_2 asymptotes to 1 as the Prandtl number decreases. It touches the outer boundary $(s_2 = 1)$ at $P \approx 0.1$, so that the WKBJ approach adopted is not completely justified for a smaller Prandtl number. Because of a large displacement of the saddle point s_0, a locality of the solution satisfied close to $s = s_0$ is no longer effectively satisfied along the real axis. Also, a strong twisting of the turning point s_t on the real axis toward the outer boundary $s = 1$ demands a larger correction than a higher-order approximation may afford in this limit.

7. Comparison with the numerical results

In this section, the results obtained in the previous section are compared with the numerical results obtained by Zhang (1992) and W. Hirsching (private communication) (see also Hirsching & Yano 1992). Note that Hirsching is using

† If the second eigensolution still remains recessive near the boundaries, a correction to satisfy appropriately the boundary conditions does not remain a small quantity. It follows that the eigensolution chosen as a leading-order solution contains an error of order unity, as do the critical parameters defined along with it. Consequently, the exchange of the dominance of the eigensolutions is crucial for the consistency of the present WKBJ approach.

		Numerical results	Asymptotics
$P = 0.1$	$R/R_b =$	4.2	3.58
	$m/m_b =$	1.6	0.96
	$\omega/\omega_b =$	0.60	0.76
$P = 1$	$R/R_b =$	1.35	1.24
	$m/m_b =$	1.23	0.99
	$\omega/\omega_b =$	1.28	1.09
$P = 10$	$R/R_b =$	1.18	1.29
	$m/m_b =$	1.47	1.15
	$\omega/\omega_b =$	1.51	1.80

TABLE 1. Comparison of the critical parameters. The numerical values are according to Zhang (1992). All the critical values are given relative to the standard values given by (4.6), originally derived by Busse (1970), apart from a correction of order σ given by (4.7).

basically the same code as Zhang. The comparison proceeds from the values of critical parameters (table 1) to the structure of the marginal modes.

It is seen in figure 3(a) that the correct critical Rayleigh number increases dramatically for a smaller Prandtl number. It asymptotes to $R \to 1.26133/P$ as $P \to 0$. The critical Rayleigh number attains its minimum value at $P \sim 1$, and slightly increases as P increases. The first row of table 1 shows a comparison of the critical Rayleigh number for the case $P = 0.1$ with Zhang's (1992) numerical results (taken from figure 1 and table 2 of Zhang 1992): the leading factors agree. A tendency of the slight departure from Busse's (1970) previous asymptotics (after the correction of (4.7)) for larger Prandtl numbers ($P = 1, 10$) is also in accordance with Zhang's numerical results. The magnitude of frequency shown in figure 3(b) is smaller for smaller Prandtl number, in qualitative agreement with figure 1 of Zhang (1992: the third row of table 1). As a whole, table 1 shows that the dependence of the critical parameters on Prandtl number is qualitatively in agreement with Zhang's (1992) recent numerical results, apart from the weaker dependence of azimuthal wavenumber m on P than Zhang's results, and a relatively large discrepancy in the critical frequencies for $P = 1, 10$.

The structure of the marginal mode is inferred from figure 5 in our results. It is seen that the tilting of the vortex columns (figure 5a) increases with decreasing Prandtl number, while the localization of the columns (figure 5b) weakens as the Prandtl number decreases. The distance s_t of the centre of the convection columns from the axis of rotation (figure 5c) has a minimum around $P \sim 1$, and increases dramatically for the smaller Prandtl number, while it shows a weak increase for a larger Prandtl number. All these characteristics are in good agreement with Zhang (1992: particularly summarized by figure 3).

Both Zhang and Hirsching's numerical results show a strong spiralling of columns (a dramatic increase of the tilting in the outward direction) for smaller Prandtl numbers. In order to compare this type of structures more closely, we have plotted both the numerical and the present asymptotic results in term of the dependence of the amplitude $A(s)$ and the phase shift $\varphi_0(s)$ on the radial distance s on the equatorial plane, defined by

$$V(s, \varphi, z = 0) = A(s) \exp[\mathrm{i}\hat{m}(\varphi - \varphi_0(s))],$$

while for the numerical results the poloidal potential has been taken for $V(s, \varphi, z)$. The results are depicted in figure 6: figure (a, b) compares the results for $\epsilon = 3.41 \times 10^{-2}$,

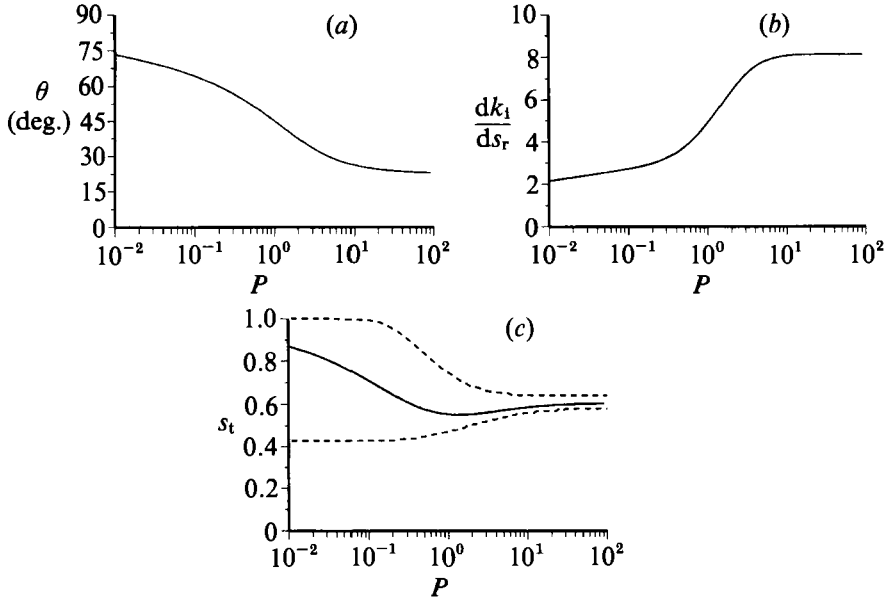

FIGURE 5. The dependence of characteristic values of the convection columns on the Prandtl number P: (a) tilting angle θ (6.8); (b) steepness $\mathrm{d}k_i/\mathrm{d}s_r$; ($c$) turning point s_t (solid curve), and the crossing points s_1, s_2 of the anti-Stokes lines with the real axis (dashed curves).

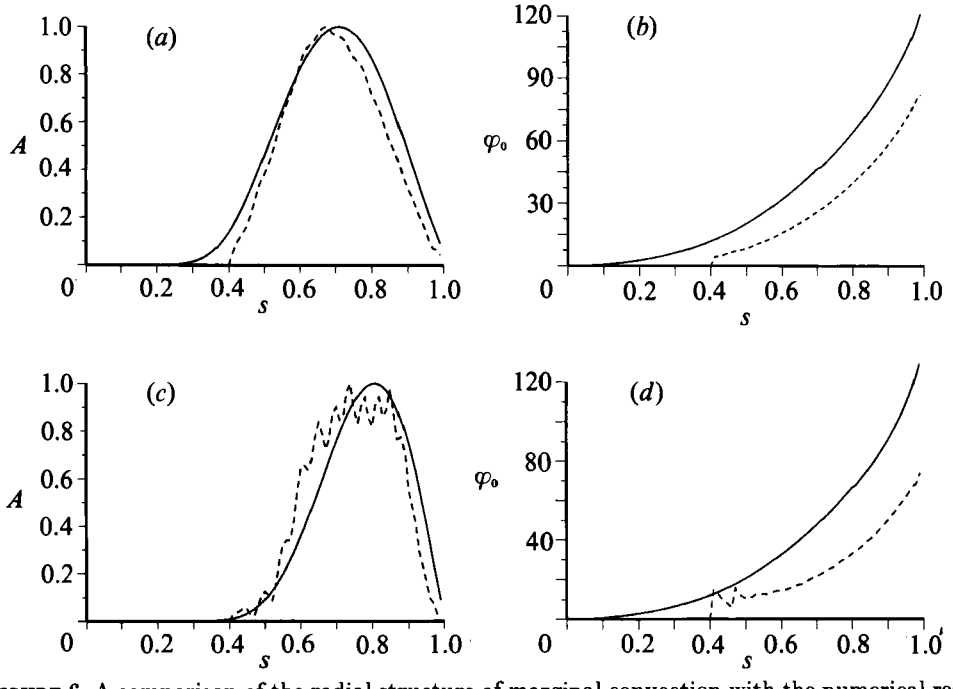

FIGURE 6. A comparison of the radial structure of marginal convection with the numerical results: (a, b) $\epsilon = 3.41 \times 10^{-2}$, $P = 0.1$, $\hat{m} = 12$ (corresponding to $T = 10^{10}$); (c, d) $\epsilon = 2.31 \times 10^{-2}$, $P = 0.03$, $\hat{m} = 22$ (corresponding to $T = 10^{12}$). (a, c) The amplitude $A(s)$; (b, d) the phase shift $\varphi_0(s)$. The results from the asymptotic theory are represented by solid curves, the numerical results by dashed curves.

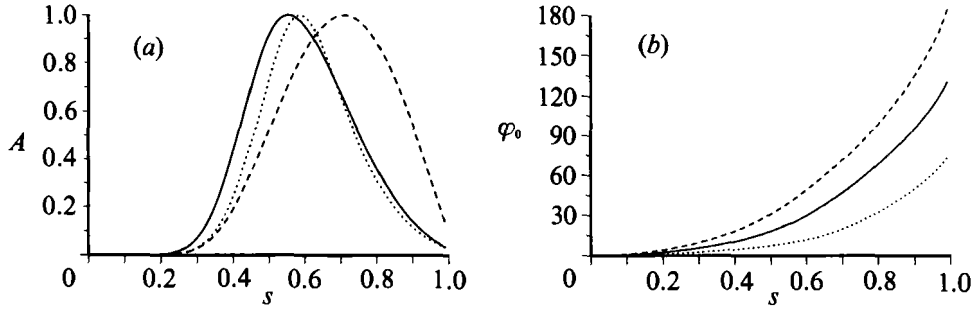

FIGURE 7. The change of the radial structure of the marginal mode with the Prandtl number P: (a) amplitude $A(s)$, (b) phase shift (spiralling) $\varphi_0(s)$ with $\epsilon = 0.1$ for the cases $P = 0.1$ (dashed line), $P = 1$ (solid line), $P = 10$ (dotted line).

$P = 0.1$, $\hat{m} = 12$ (corresponding to the Taylor number $T = 10^{10}$ in Zhang's (1992) definition); figure 6(c, d) compares the results for $\epsilon = 2.31 \times 10^{-2}$, $P = 0.03$, $\hat{m} = 22$ (corresponding to $T = 10^{12}$). Figure 6(a, c) shows the amplitude $A(s)$, while figure 6(b, d) shows the phase shift $\varphi_0(s)$. The solid lines are asymptotic results computed from the complex radial wavenumbers $k(s)$ as shown in figure 4(a, b), while the dashed curves are Hirsching's numerical results. The agreement is particularly good for $P = 0.1$, while a relatively large disagreement of the phase shift is noticeable for $P = 0.03$. The asymptotics of the anti-Stokes line to $s = 1$ predict a less accurate result for a smaller Prandtl number $P < 0.1$.

The structure of the modes expected from our asymptotic theory is summarized in figure 7 for the cases $P = 0.1$, 1, 10 with $\epsilon = 0.1$. The steepening of Taylor columns weakens dramatically for the smaller Prandtl number $P = 0.1$ (figure 7a), while the spiralling increases dramatically as the Prandtl number decreases from $P = 10$ to 0.1 (figure 7b). The results agree well with the recent numerical results by both Zhang and Hirsching. The present asymptotic theory shows that the columnar mode that appears with a large Prandtl number continuously modulates into a strongly spiralling mode at a smaller Prandtl number. On the other hand, even though the isolation of Taylor columns seems numerically extremely weak for spiralling modes of smaller Prandtl numbers, the present result predicts that it is, nevertheless, confined to a boundary layer of $O((E/P)^{\frac{1}{3}})$ asymptotically. A much higher Taylor number is required to confirm this prediction numerically. Also note that since the boundary layer widens for smaller Prandtl numbers with a fixed Ekman number, such a numerical setting leads to the illusion that the asymptotic theory has been nullified.

8. Discussion

Three convection modes have been identified by numerical studies of rapidly rotating self-gravitating systems (Zhang & Busse 1987; Zhang 1992; Hirsching, private communication): the columnar, the spiralling, and the wall-attached modes. The analysis of the previous section reveals that the columnar and the spiralling modes constitute the same branch in phase space, with a continuous modulation from one to the other as the Prandtl number decreases. On the other hand, the preliminary analysis in Appendix C suggests that the wall-attached mode can be identified as an inertial Airy-function-type mode.

The easiest starting point to understand the mechanism that leads to different

dynamical regimes (columnar, spiralling, wall-attached) is to examine the wave dispersion of the system, which can be written

$$\omega = \frac{(1+P)\eta^*}{\alpha^2} + imP\left(m^2\alpha^2 - \frac{R}{\alpha^2}\frac{\Theta}{V}\right) \tag{8.1}$$

from (3.2), by implicitly assuming the possibility of a complex wavenumber α. It is seen that in the limit $P \to 0$ the dispersion relationship (8.1) tends to a simple Rossby wave dispersion relationship given by (4.1*b*) as long as $R \sim O(1)$ is assumed. In this limit, the diffusivity plays no part in the dispersion relation. Consequently, only the oscillatory mode is possible in this limit with this scaling. The regime corresponds to the inertial (wall-attached) mode considered in Appendix C.

On the other hand, with a finite effect of Prandtl number P, which measures the magnitude of kinematic diffusivity, it is seen from (8.1) that a complex wavenumber α is allowable, which enables a strongly isolated columnar mode to appear at a higher Prandtl number (see figures 5*b*, 7*a*). In order to realize a columnar mode even in the limit $P \to 0$, by retaining the second term of the dispersion relation (8.1), which allows a complex wavenumber α, we have to invoke a strong buoyancy force of $R \sim (1/P)$. As a result, the thermal diffusivity effectively acts to isolate the columns in the vorticity equation (3.2). In mathematical terms, this is equivalent to requiring a large shift of the turning point s_0 from the real axis, which causes a strong spiralling in physical space (figures 5*a*, 7*b*). In physical terms, while the isolation of convection requires a strong buoyancy force in order to invoke an effective thermal diffusivity, there is no effective kinematic diffusivity to counterbalance the buoyancy force, as in the case of $P > O(1)$. Consequently, a fluid particle accelerated by the buoyancy force overshoots away from the kinematic diffusive boundary layer. Since the fluid particle senses a local phase velocity, which increases in magnitude with distance s, the fluid particle ends up with a strongly elongated closed streamer, represented by a spiralling pattern. Note that such a deformation is also preferable in respect of transportation of heat for a longer distance by a single fluid particle.

On the other hand, in the limit of a very large Prandtl number, $P \to \infty$, the balance is essentially achieved within the second term of (8.1): the buoyancy force (the second part) is effectively balanced by the kinematic diffusivity (the first part). Consequently, in this case, without any overshooting, the fluid is confined to a kinematic diffusive boundary layer. As a result, the convection columns are steep and do not experience much deformation in the radial direction.

Remember that the radial scale is order of ϵ, which is measured in terms of both the kinematic diffusivity ν and the thermal diffusivity κ as

$$\epsilon \sim \begin{cases} \nu^{\frac{1}{3}}, & P \to \infty \\ \kappa^{\frac{1}{3}}, & P \to 0. \end{cases}$$

This scaling also supports the above argument that convection is characterized by a thermally diffusive boundary layer with $P \to 0$ and a kinematically diffusive boundary layer as $P \to \infty$.

The dimensional critical temperature gradient β (defined by (2.1*b*)), which initiates thermal convection, also suggests how the underlying physics might be understood (e.g. Soward 1977). It is directly inferred from the scaling of the Rayleigh number (2.7*a*). In the limit of a large Prandtl number, the critical temperature gradient is scaled as

$$\beta \sim \kappa\nu^{-\frac{1}{3}}$$

in terms of kinematic and thermal diffusivities. It is observed that a larger kinematic diffusivity helps to initiate convection, which is realized as a kinematic boundary layer. On the other hand, thermal diffusivity acts as a hindering factor to initiate marginal convection in this limit.

However, when we inspect the limit of small Prandtl number for the columnar-spiralling mode, we obtain the scaling

$$\beta \sim \kappa^{\frac{2}{5}}$$

from the ordering $PR \sim 1$. In this limit, the kinematic diffusivity plays no role in initiating convection, while thermal diffusivity acts as a suppressing factor. This is a very ironical situation, because as the columnar mode modulates into the spiralling mode, the convection layer modules from a kinematic one to thermal one. Obviously, the thermal diffusion plays a crucial role in isolating the convection columns in this limit. However, in order to corporate the effect of thermal diffusivity into the dynamics, a sufficiently large temperature gradient must be invoked for the purpose.

In contrast, the critical temperature gradient for the inertial Airy-function-type mode (wall-attached mode) is measured by

$$\beta \sim \nu\kappa^{-\frac{2}{3}}$$

from the scaling $\epsilon R \sim 1$ (Appendix C). The role of kinematic and thermal diffusivities is reversed from that of the columnar mode in the limit of $P \to \infty$. Since the inertial mode is characterized by an almost inviscid neutral oscillatory motion, the existence of kinematic viscosity acts as a hindering factor, while in contrast to the spiralling mode, a large thermal diffusivity helps to initiate marginal convection.

9. Concluding remarks

A revised asymptotic theory of thermal convection in rapidly rotating systems has been constructed for cases applicable both to geophysical self-gravitating systems and their laboratory analogues, where the centrifugal force mimics self-gravitation. A conventional WKBJ approach (Busse 1970) assuming local real wavenumbers is not applicable to this system, because the spatial wave dispersion of the solution leads to an exponential blow up of the modulation at a higher order (Soward 1977). The difficulty is avoided by seeking a virtual centre of convection on a complex plane, where the wave dispersion locally disappears. The point is identified as a saddle point of the critical Rayleigh number on the complex plane.

The result leads to a larger critical Rayleigh number than that of the previous conventional approach (Busse 1970). Nevertheless, the correction is just a factor of up to 1.3 for large Prandtl numbers ($P > 1$), and a qualitative feature of convection obtained in the present study basically confirms the view inferred in the previous studies (namely Roberts 1968; Busse 1970).

On the other hand, the critical Rayleigh number increases proportional to the inverse of Prandtl number as $P \to 0$ relative to the previous value. This large discrepancy with the previous asymptotic theory is, in mathematical terms, caused by the need to shift the virtual centre of convection for a larger distance from the real axis in the limit of small Prandtl numbers. In physical terms, the internal boundary layer sustaining the convective Taylor columns transforms into a thermally diffusive boundary layer from a kinematic diffusive boundary layer with decreasing Prandtl number. Consequently, in order to overcome a large thermal diffusivity within the boundary layer, a larger temperature gradient must be imposed than estimated from previous asymptotic theory.

A qualitative feature of convection obtained in the present study basically confirms the view inferred in the previous studies (namely Roberts 1968; Busse 1970). However, a main quantitative difference in the present results is the radial scale. It has been estimated as $O(E^{\frac{2}{5}})$ (Roberts 1968), which is much longer than that of the azimuthal direction. The present revised asymptotic theory shows that the actual radial scale is as small as the azimuthal scale (i.e. $O(E^{\frac{1}{3}})$). The deformation (or spiralling) of convection columns has been inferred as a higher-order perturbation in the previous studies (e.g. Busse 1983; Busse & Hood 1982). The present asymptotic analysis reveals that the scale of deformation of convection columns is of the same order as that of the convection columns themselves. Both of the them have been described in terms of the complex radial wavenumber. In particular, a continuous modification from the columnar modes to the spiralling modes is vividly demonstrated in terms of the phase shifting of the convection columns in the radial direction (figure 7*b*), which is one of the main improvements obtained by the present revised asymptotic theory.

It is also found that in the limit of small Prandtl number a competitive mode helped by a large thermal diffusivity appears. This mode, described as an almost neutral inertial oscillation, is expected to correspond to the wall-attached mode identified in the numerical study of Zhang & Busse (1987). A preliminary analysis for this mode is performed in Appendix C. An approximate transition diagram from the columnar-spiralling mode to the inertial mode is drawn. A more careful analysis for this mode is still to be done.

The present analysis has been restricted to the limit of weak inclination of the outer boundaries relative to the equatorial plane. The analysis has been remarkably simplified by this approximation, because the dependence of the solutions on the direction of the axis of rotation no longer needs to be considered explicitly. It should be emphasized that the previous analysis by Busse (1970) demonstrates the usefulness of this limit. He has shown that, in terms of the previous asymptotic theory, the results with this approximation agree well with a full spherical analysis, which solves the z-dependence of the problem explicitly. In Appendix A, it is shown that the agreement further improves by considering a first-order correction to a weak-inclination analysis. This approximation is expected to be still valid, even in terms of the present revised analysis, as long as a deviation of the critical distance s_0 from the real axis and, subsequently, a correction of Rayleigh number are small enough. Since both corrections are small for a large Prandtl number, the result obtained for this limit is of good accuracy in this parameter range. On the other hand, because of a large shifting of the distance s_0 to a complex plane and a diverging correction to the Rayleigh number, the solution is qualitatively different from Busse's (1970) analysis for smaller Prandtl numbers. Nevertheless, the analysis of Appendix A implies that the analysis can be considered as a leading-order result in terms of a formal weak-inclination expansion approach. Higher-order corrections due to a finite boundary inclination can be computed by proceeding to a higher order of expansion of σ. In this respect, even for smaller Prandtl numbers, the approximate results are expected to be a qualitatively good representation. As remarked at the end of §3, the extension of the present analysis to the full spherical problem is, in principle, quite straightforward. However, the actual procedure is extremely involved, because we have to solve the z-dependence of the problem at each point on a complex plane, as we survey the saddle point. Note that, since the boundary condition (2.10) can be satisfied only locally in the full spherical problem, we have to supply a solvability condition corresponding to (3.7) at the turning point s_t, which

should in turn be identified as a consequence of a complex plane analysis. An analysis in terms of a σ-expansion may offer a short-cut to solving the problem.

The qualitative nature of the present analysis should be emphasized. A physical structure of convection in a high rotation limit is elucidated by surveying a wide range of parameters. By adopting a general formulation of the problem, it is also shown that the structure of the problem is inherent in every rotating system of this type which contains a non-vanishing curvature on its outer boundaries. For this reason, the laboratory analogues proposed by Busse (1970) can be used to demonstrate this peculiar behaviour of instabilities by experiments. Even though all the numerical results have been presented in terms of the spherical geometry, the algebraic formulation presented is readily applied to any geometrical boundaries fit to the settings of the laboratory rotating systems.

The beginning of the present work can be traced to a conversation with Andrew Soward during the summer Study Programme of Geophysical Fluid Dynamics at Woods Hole, MA in July 1987. The actual start of the work has been enabled by Fritz H. Busse, who invited me to Bayreuth under the Alexander von Humboldt Research Fellowship for June 1990–October 1991. I express my sincere thanks for his continuous encouragements and a few, but very decisive, suggestions. In particular, he pushed me to concentrate on the limit of weak inclinations of the outer boundaries. I also thank the Alexander von Humboldt Foundation, for providing me a German course under the fellowship, which enabled German discussions with Wolfram Hirsching, who also has kindly given me his unpublished numerical results. An intensive discussion with Andrew Soward and Chris Jones in May 1991 was helpful to complete the work. Sergio Cordero read the manuscript very carefully for me during completion of the final draft.

Appendix A. A higher-order correction for the effects of the inclination of the outer boundary

The order-σ corrections for the leading-order results in the main text based on (3.1*c*) and (3.2) are considered in this Appendix. The higher-order terms in ϵ in (2.9) will still be neglected. All the quantities are expanded in terms of σ:

$$V = V_0+\sigma V_1+\ldots, \quad W = W_0+\sigma W_1+\ldots, \quad \Theta = \Theta_0+\sigma\Theta_1+\ldots,$$

and

$$R = R_0+\sigma R_1+\ldots, \quad \omega = \omega_0+\sigma\omega_1+\ldots,$$

where R_0 and ω_0 refer to the critical parameters defined in §4 or §6.

The z-component W_0 of the velocity at leading order is defined by

$$W_0 = \eta^* V_0 z \tag{A 1}$$

from the consistency of (3.1*a*) and (3.2).

The $O(\sigma)$ problem is defined by

$$(\omega_0+\mathrm{i}m^3P\Delta^*)\,\Delta^*V_1+(1+P)\,(\partial W_1/\partial z)-\mathrm{i}mPR_0\,\Theta_1+\omega_1\,\Delta^*V_0-\mathrm{i}mPR_1\,\Theta_0 = 0, \tag{A 2a}$$

$$(1+\mathrm{P})\,(\partial/\partial z)\,\Delta^*V_1+\mathrm{i}mPR_0\,\lambda z\Delta^*\Theta_0 = 0, \tag{A 2b}$$

$$(\omega_0+\mathrm{i}m^3\Delta^*)\,\Theta_1+\mathrm{i}mV_1+\omega_1\,\Theta_0+\mathrm{i}m\lambda z\,W_0 = 0 \tag{A 2c}$$

from (2.9). Equation(A 2*b*) defines V_1 as

$$V_1 = V_1(0)-\frac{\mathrm{i}mPR_0}{2(1+P)}\lambda z^2\Theta_0. \tag{A 3}$$

Equations (A 1) and (A 3) imply that V and W are even and odd functions of z, respectively. By integrating (A 2a) and (A 2b) in the z-direction from $-\eta_b$ to η_b, respectively, we obtain, by taking into account the boundary condition (2.10),

$$[(\omega_0+\mathrm{i}m^3P\Delta^*)\Delta^*+(1+P)\eta^*]\bar{V}_1-\mathrm{i}mPR_0\bar{\Theta}_1+\omega_1\Delta^*V_0-\mathrm{i}mP(\tfrac{1}{3}\lambda\eta^*\eta_b^2R_0+R_1)\Theta_0=0, \tag{A 4a}$$

$$(\omega_0+\mathrm{i}m^3\Delta^*)\bar{\Theta}_1+\mathrm{i}m\bar{V}_1+\omega_1\Theta_0+\tfrac{1}{3}\mathrm{i}m\lambda\eta^*\eta_b^2V_0=0, \tag{A 4b}$$

where the bar denotes the average in the z-direction. The corrections R_1, ω_1, to the parameters are defined by a solvability condition, which is given by multiplying V_0 and Θ_0 by (A 4a) and (A 4b), respectively, and taking their sum, integrated in the s-direction from 0 to 1:

$$\frac{\langle V_0\Delta^*V_0\rangle-PR_0\langle\Theta_0^2\rangle}{\langle V_0\Theta_0\rangle}w_1+\mathrm{i}mP\left[\frac{2}{3}\lambda\frac{\langle-\eta^*\eta_b^2V_0\Theta_0\rangle}{\langle V_0\Theta_0\rangle}R_0-R_1\right]=0, \tag{A 5}$$

where $\langle\cdot\rangle$ denotes integration in the s-direction. In performing the partial integrations, it has been assumed that V_0 and Θ_0 tend to vanish toward $s=0$, 1. Note that the spherical geometry satisfying (2.6b) and (4.5) gives

$$-\eta^*\eta_b^2=1.$$

Consequently, we obtain

$$\omega_1=0, \quad R_1=\tfrac{2}{3}\lambda R_0 \tag{A 6a,b}$$

for the spherical geometry. Recall that λ measures the magnitude of the gravitational force in the direction parallel to the axis of rotation.

Appendix B. The role of wave dispersion

The spatial dispersion of the wave is given by

$$\frac{\partial\omega}{\partial s_r}=-\frac{\partial\hat{\mathscr{L}}_i/\partial s_r}{\partial\hat{\mathscr{L}}_i/\partial\omega} \tag{B 1}$$

from (6.3a). On the other hand, the Cauchy–Rieman relation implies

$$\frac{\partial\hat{\mathscr{L}}_r}{\partial s_i}=-\frac{\partial\hat{\mathscr{L}}_i}{\partial s_r}=-\mathrm{Im}\left[\frac{\partial\hat{\mathscr{L}}}{\partial s}\right]. \tag{B 2}$$

From (6.3b), (B 1), and (B 2) we conclude that when $\partial R/\partial s_i\neq0$ the wave is dispersive spatially, and vice versa.

Appendix C. The limit of small Prandtl number

In this Appendix, we offer a preliminary analysis for the Airy-function-type mode that appears in the limit of small Prandtl number. For simplicity, we assume the inequality

$$1\gg P\gg\sigma,\epsilon^2$$

and neglect the higher-order terms in both σ and ϵ throughout the analysis. The Laplacian is approximated by

$$\Delta^*\approx-(1/s^2)+(\epsilon^2/m^2)(\partial^2/\partial s^2),$$

by implicitly assuming $\partial/\partial s \sim \epsilon^{-1}$. All the quantities are expanded in Prandtl number P, e.g.

$$V = V^{(0)} + PV^{(1)} + \ldots, \quad \omega = \omega^{(0)} + P\omega^{(1)} + \ldots, \quad R = R^{(0)} + PR^{(1)} + \ldots.$$

At leading-order in Prandtl number, (3.2) reduces to an equation for the inertial oscillation

$$[(\partial^2/\partial s^2) + (m^2/\epsilon^2) f(s)] V^{(0)} = 0, \tag{C 1}$$

where

$$f(s) \equiv (\eta^*(s)/\omega^{(0)}) - (1/s^2).$$

The square $f(s)$ of the local radial wavenumber contains a single first-order turning point, say, s_0, such that $f(s)$ is negative at $s < s_0$ and positive at $s > s_0$. Consequently, the inertial wave is evanescent inside turning distance $s = s_0$ and is of standing wave character outside the cylinder $s = s_0$. The leading-order expression for the asymptotic expansion in the limit $\epsilon \to 0$ (see e.g. Olver 1974, Ch. 11) is given by

$$V^{(0)} = (\zeta/f(s))^{\frac{1}{4}} \mathrm{Ai}(-(m/\epsilon)^{\frac{2}{3}}\zeta) \tag{C 2}$$

in terms of the Airy function $\mathrm{Ai}(z)$. Here the radial distance s has been transformed into ζ by

$$\zeta = \begin{cases} \dfrac{3}{2}\left[\displaystyle\int_{s_0}^{s} f^{\frac{1}{2}}(s')\,\mathrm{d}s'\right]^{\frac{2}{3}}, & s > s_0 \\ -\dfrac{3}{2}\left[\displaystyle\int_{s}^{s_0} [-f(s')]^{\frac{1}{2}}\,\mathrm{d}s'\right]^{\frac{2}{3}}, & s < s_0. \end{cases}$$

The leading-order temperature $\Theta^{(0)}$ is then defined by (3.1 *c*). Note that for a spherical problem with (4.5) the turning point s_0 is related to the frequency $\omega^{(0)}$ by

$$\omega^{(0)} = -s_0^2/(1-s_0^2).$$

As a boundary condition, we assume

$$V^{(0)} = 0$$

at $s = 1$, which is equivalently stated by

$$\xi_j = -(m/\epsilon)^{\frac{2}{3}}\zeta(s = 1), \tag{C 3}$$

where ξ_j is the jth zero (in ascendent order) of the Airy function. It follows that the solution contains j nodes in the radial direction, when ξ_j is taken as an eigenvalue of the solution. From the characteristic structure of the Airy function, it is inferred that the solution is reminiscent of the wall-attached mode, numerically detected by Zhang & Busse (1987). Also note that the asymptotic parameter ϵ is explicitly related to the zero ξ_j of the Airy function by (C 3). Consequently, we require the explicit value of the parameter ϵ to obtain the final results.

At the first order of Prandtl number, we obtain

$$(\omega^{(0)}\Delta^* + \eta^*) V^{(1)} + [(\omega^{(1)} + im^3\Delta^*)\Delta^* + \eta^*] V^{(0)} - imR^{(0)}\Theta^{(0)} = 0 \tag{C 4}$$

from (3.2). A solvability condition for (C 4) is obtained by multiplying $V^{(0)}$ by (C 4) and by integrating it in the s-direction from 0 to 1. After some manipulations, the eigenvalues are defined by

$$R^{(0)} = \frac{1}{m^2\omega^{(0)3}} \langle \eta^{*2} V^{(0)2} \rangle \left\langle \frac{\eta^* V^{(0)2}}{\omega^{(0)4} + m^6\eta^{*2}} \right\rangle^{-1}, \tag{C 5a}$$

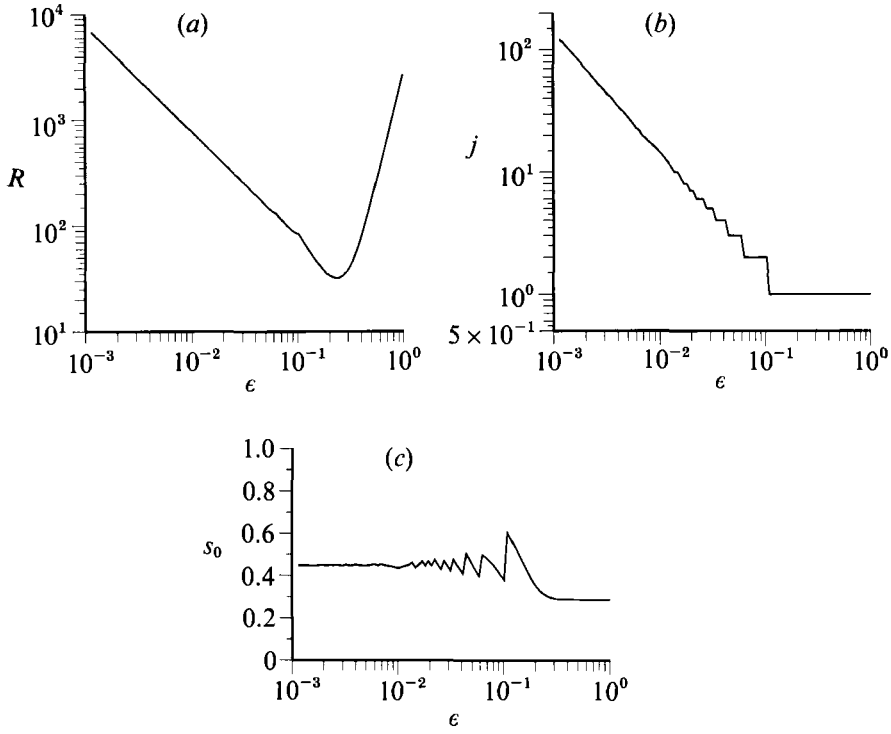

FIGURE 8. (*a*) The critical Rayleigh number R (*b*) the eigenmode j, and (*c*) for the turning point s_0, of the inertial mode as a function of the parameter ϵ.

$$\left(1-\frac{\omega^{(1)}}{\omega^{(0)}}\right) = m^2\omega^{(0)3}R^{(0)}\langle\eta^* V^{(0)2}\rangle^{-1}\left\langle\frac{V^{(0)2}}{\omega^{(0)4}+m^6\eta^{*2}}\right\rangle, \tag{C5b}$$

where $\langle\cdot\rangle$ denotes integration in the s-direction.

The critical Rayleigh number $R^{(0)}$ is calculated numerically by using (C5*a*). The minimum is sought in terms of the order j of the zero ξ_j. The dependence of the critical Rayleigh number $R^{(0)}$ and the eigenmode j on the parameter ϵ are depicted in figures 8(*a*) and 8(*b*) respectively. The corresponding turning point s_0 is shown in figure 8(*c*).

Both the critical Rayleigh number $R^{(0)}$ and the number of nodes j increase with the inverse of ϵ as ϵ decreases. Since the radial scale decreases proportionally as ϵ decreases, the tuning point s_0 is always adjusted to about midway from the axis of rotation by increasing the mode j. It is shown that the frequency ω asymptotes to -0.25, identical to the standard value (4.6*b*), while the critical azimuthal wavenumber asymptotes to 0.0225 as $\epsilon\to0$, a value smaller than that of the standard value given by (4.6*c*). The scaling of (2.7*a*) implies that the Rayleigh number increases as $\sim\sigma^{\frac{4}{3}}\sim\epsilon^{-\frac{8}{9}}\approx\epsilon^{-1}$, by taking the effective inclination of the boundary as $\sigma\sim\epsilon^{-\frac{2}{3}}$, because the position of the strongest columns attached to the equatorial boundary is measured by $1-s\sim\epsilon^{\frac{2}{3}}$. The result is consistent with this scaling.

The transition point from the spiralling modes to the wall-attached mode may be estimated in the following way. It has been observed that the critical Rayleigh number of the spiralling mode tends to

$$R = 1.26133/P \tag{C6}$$

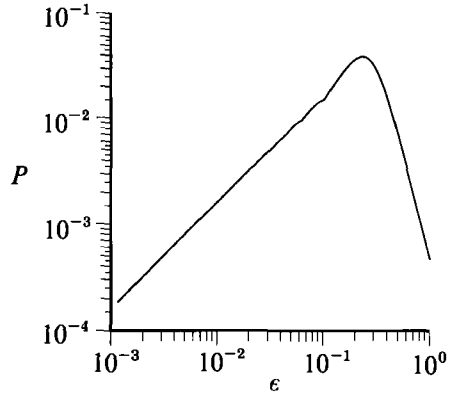

FIGURE 9. The transition diagram from the spiralling mode (upper left) to the wall-attached mode (lower light).

as $P \to 0$. Consequently, the critical Prandtl number P_c, where the transition occurs at a given parameter ϵ (measures the Ekman number), is obtained by equating the two expressions (C 5*a*) and (C 6) for the Rayleigh number, namely,

$$P_c(\epsilon) = 1.26133/R^{(0)}(\epsilon).$$

The result is depicted in figure 9. Since the critical Rayleigh number of the wall-attached mode increases inversely to ϵ, it is seen that the transition Prandtl number P_c also decreases proportionally as ϵ decreases. The result qualitatively agrees with the phase diagram inferred by Zhang & Busse (1987) numerically.

Appendix D. Mathematical notes

The condition $\delta R/\delta s_0 = 0$ is equivalent to (4.2*c*) along the real axis, and is equivalent to (6.1*b*) on the complex plane of s_0. These are established as follows.

D.1. *Equivalence of* $\partial R/\delta s_0 = 0$ *to* (4.2*c*)

By recalling the definition of $\delta R/\delta s_0$ and the relation (B 1), we have

$$\frac{\delta R}{\delta s_0} = \frac{1}{m^2 P}\left[\frac{\partial \hat{\mathscr{L}}_r}{\partial s_0}\frac{\partial \hat{\mathscr{L}}_i}{\partial \omega} - \frac{\partial \hat{\mathscr{L}}_r}{\partial \omega}\frac{\partial \hat{\mathscr{L}}_i}{\partial s_0}\right] \Big/ \frac{\partial \hat{\mathscr{L}}_i}{\partial \omega}. \tag{D 1}$$

On the other hand, (4.2*c*) is equivalent to

$$\mathrm{Im}\left[\left(\frac{\partial \hat{\mathscr{L}}_r}{\partial s_0} + \mathrm{i}\frac{\partial \hat{\mathscr{L}}_i}{\partial s_0}\right)\left(\frac{\partial \hat{\mathscr{L}}_r}{\partial \omega} - \mathrm{i}\frac{\partial \hat{\mathscr{L}}_i}{\partial \omega}\right)\right] = 0. \tag{D 2}$$

When the derivation of s_0 is restricted along the real axis, the equivalence of (D 2) to (D 1) is obtained by explicitly extracting the imaginary components in (D 2).

D.2. *Equivalent of* $\delta R/\delta s_0 = 0$ to (6.1*b*)

When the analysis is extended to a complex s_0, the condition (D 1) is stated equivalently by

$$\frac{\partial \hat{\mathscr{L}}_r}{\partial s_r}\frac{\partial \hat{\mathscr{L}}_i}{\partial \omega} - \frac{\partial \hat{\mathscr{L}}_i}{\partial s_r}\frac{\partial \hat{\mathscr{L}}_r}{\partial \omega} = 0, \quad \frac{\partial \hat{\mathscr{L}}_r}{\partial s_i}\frac{\partial \hat{\mathscr{L}}_i}{\partial \omega} - \frac{\partial \hat{\mathscr{L}}_i}{\partial s_i}\frac{\partial \hat{\mathscr{L}}_r}{\partial \omega} = 0$$

or by further employing the Cauchy–Rieman relations,

$$\frac{\partial \hat{\mathscr{L}}_r}{\partial s_r}\frac{\partial \hat{\mathscr{L}}_i}{\partial \omega}+\frac{\partial \hat{\mathscr{L}}_r}{\partial s_i}\frac{\partial \hat{\mathscr{L}}_r}{\partial \omega}=0, \quad \frac{\partial \hat{\mathscr{L}}_r}{\partial s_i}\frac{\partial \hat{\mathscr{L}}_i}{\partial \omega}-\frac{\partial \hat{\mathscr{L}}_r}{\partial s_r}\frac{\partial \hat{\mathscr{L}}_r}{\partial \omega}=0. \tag{D 3a,b}$$

As long as $(\partial \hat{\mathscr{L}}_r/\partial\omega)^2+(\partial \hat{\mathscr{L}}_i/\partial\omega)^2 \neq 0$, the equivalence of (D 3a,b) to (6.1b) is supported by (4.3d).

D.3. *Identification of a saddle point as a critical distance* s_0

In seeking a complex radial distance s_0, where the maximum amplitude of convection is attained, a graphical approach has been made on figure 1. An implicit assumption of this graphical approach is the identification of the critical point as a saddle point defined by the relation

$$\frac{\mathrm{d}R}{\mathrm{d}s}\equiv\frac{\partial R}{\partial s}+\frac{\partial R}{\partial \omega}\left(\frac{\partial \omega}{\partial s}+\frac{\partial \omega}{\partial m}\frac{\partial m}{\partial s}+\frac{\partial \omega}{\partial k}\frac{\partial k}{\partial s}\right)+\frac{\partial R}{\partial m}\frac{\partial m}{\partial s}+\frac{\partial R}{\partial k}\frac{\partial k}{\partial m}=0. \tag{D 4}$$

Note that the condition (D 4) is equivalent to the following set of conditions:

$$\frac{\partial R}{\partial s}+\frac{\partial R}{\partial \omega}\frac{\partial \omega}{\partial s}=0, \quad \frac{\partial R}{\partial m}+\frac{\partial R}{\partial \omega}\frac{\partial \omega}{\partial m}=0, \quad \frac{\partial R}{\partial k}+\frac{\partial R}{\partial \omega}\frac{\partial \omega}{\partial k}=0, \tag{D 5a–c}$$

as long as $\partial m/\partial s \neq 0$ and $\partial k/\partial s \neq 0$.

The equivalence of (D 5a) to (6.1b) has been established in the previous section. The equivalence of (D 5a,b) to (4.2a,b), respectively, is readily proved in a similar manner. Consequently, the set of conditions (4.2a,b), (6.1b) is equivalent to identifying a saddle points with (D 4) of Rayleigh number on the complex s_0-plane. Note that in the actual procedure, the condition (D 5c) is satisfied from the outset by setting $k = 0$. Also note that the Rayleigh number minimum in respect to m has been plotted on every point of the complex plane in figure 1, which satisfies (D 5b).

It is also possible to repeat a similar procedure for a fixed azimuthal wavenumber m. This actually corresponds to the procedure used by Zhang (1992) to identify the marginal mode numerically. An equivalent statement to (D 4) in this case is

$$\left(\frac{\mathrm{d}R}{\mathrm{d}s}\right)_m\equiv\frac{\partial R}{\partial s}+\frac{\partial R}{\partial \omega}\frac{\partial \omega}{\partial s}+\left(\frac{\partial R}{\partial k}+\frac{\partial R}{\partial \omega}\frac{\partial \omega}{\partial k}\right)\frac{\partial k}{\partial s}=0.$$

Even in this case, the identical result is recovered finally by choosing m such that (D 5b) is satisfied at a saddle point.

REFERENCES

Busse, F. H. 1970 Thermal instabilities in rapidly rotating systems. *J. Fluid Mech.* **44**, 441–460.

Busse, F. H. 1983 A model of mean zonal flows in the major planets. *Geophys. Astrophys. Fluid Dyn.* **23**, 153–174.

Busse, F. H. 1986 Asymptotic theory of convection in a rotating cylindrical annulus. *J. Fluid Mech.* **173**, 545–556.

Busse, F. H. & Carrigan, C. R. 1976 Laboratory simulation of thermal convection in rotating planets and stars. *Science* **191**, 81–83.

Busse, F. H. & Hood, L. L. 1982 Differential rotation driven by convection in a rapidly rotating annulus. *Geophys. Astrophys. Fluid Dyn.* **21**, 59–74.

Carrigan, C. R. & Busse, F. H. 1983 An experimental and theoretical investigation of the onset of convection in rotating spherical shells. *J. Fluid Mech.* **126**, 287–305.

CHANDRASEKAHR, S. 1961 *Hydrodynamic and Hydromagnetic Instability.* Clarendon.

GREENSPAN, H. P. 1968 *The Theory of Rotating Fluids.* Cambridge University Press.

HIRSCHING, W. R. & YANO, J.-I. 1992 Metamorphosis of marginal thermal convection in rapidly rotating self-gravitating spherical shells. *Geophys. Astrophys. Fluid Dyn.* (submitted).

HUERRE, P. & MONKEWITZ, P. A. 1990 Local and global instabilities in spatially developing flows. *Ann. Rev. Fluid Mech.* **22**, 473–537.

INGERSOLL, A. P. & POLLARD, D. 1982 Motion in the interior and atmospheres of Jupiter and Saturn: Scale analysis, anelastic equations, barotropic stability criterion. *Icarus* **52**, 62–80.

KAWAHARA, T. 1973 The derivative-expansion method and non-linear dispersive waves. *J. Phys. Soc. Japan* **35**, 1537–1544.

MILLER, J. C. P. 1950 On the choice of standard solutions for a homogeneous linear differential equation of the second order. *Q. J. Mech. Appl. Maths*, **3**, 225–235.

OLVER, F. W. J. 1974 *Asymptotics and Special Functions.* Academic.

PEDLOSKY, J. 1987 *Geophysical Fluid Dynamics*, 2nd edn. Springer.

ROBERTS, P. H. 1968 On the thermal instability of a rotating fluid sphere containing heat sources. *Phil. Trans. R. Soc. Lond.* A **263**, 93–117.

SOWARD, A. M. 1977 On the finite amplitude instability of a rotating fluid sphere. *Geophys. Astrophys. Fluid Dyn.* **9**, 19–74.

SOWARD, A. M. & JONES, C. A. 1983 The linear stability of the flow in the narrow gap between two concentric rotating spheres. *Q. J. Mech. Appl. Maths* **36**, 19–42.

ZHANG, K. K. 1992 Spiralling columnar convection in rapidly rotating spherical fluid shells. *J. Fluid Mech.* **236**, 535–556.

ZHANG, K. K. & BUSSE, F. H. 1987 On the onset of convection in rotating spherical shells. *Geophys. Astrophys. Fluid Dyn.* **39**, 119–147.